

Advances in Applied Ceramics

Structural, Functional and Bioceramics

ISSN: 1743-6753 (Print) 1743-6761 (Online) Journal homepage: <https://www.tandfonline.com/loi/yaac20>

A review of cold sintering processes

Salvatore Grasso, Mattia Biesuz, Luca Zoli, Gianmarco Taveri, Andrew I. Duff, Daoyao Ke, Anna Jiang & Michael J. Reece

To cite this article: Salvatore Grasso, Mattia Biesuz, Luca Zoli, Gianmarco Taveri, Andrew I. Duff, Daoyao Ke, Anna Jiang & Michael J. Reece (2020) A review of cold sintering processes, Advances in Applied Ceramics, 119:3, 115-143, DOI: [10.1080/17436753.2019.1706825](https://doi.org/10.1080/17436753.2019.1706825)

To link to this article: <https://doi.org/10.1080/17436753.2019.1706825>



© 2020 The Author(s). Published by Informa UK Limited, trading as Taylor & Francis Group



Published online: 16 Jan 2020.



Submit your article to this journal [↗](#)



Article views: 320



View related articles [↗](#)



View Crossmark data [↗](#)

REVIEW



A review of cold sintering processes

Salvatore Grasso^a, Mattia Biesuz^a, Luca Zoli^b, Gianmarco Taveri^c, Andrew I. Duff^d, Daoyao Ke^a, Anna Jiang^a and Michael J. Reece^e

^aKey Laboratory of Advanced technologies of Materials, Ministry of Education, School of Materials Science and Engineering, Southwest Jiaotong University, Chengdu, People's Republic of China; ^bCNR-ISTEC, Institute of Science and Technology for Ceramics, Faenza, Italy; ^cInstitute of Inorganic Chemistry, Slovak Academy of Sciences, Dúbravská cesta, Bratislava, Slovakia; ^dSTFC Daresbury Laboratory, Daresbury, UK; ^eQueen Mary, University of London, London, UK

ABSTRACT

The need to reduce the energy consumed and the carbon footprint generated by firing ceramics has stimulated research to develop consolidation techniques operating at lower temperatures, ideally not exceeding 300 °C. This has been realised in Ultra Low Energy Sintering (ULES) using high pressure (hundreds of MPa) in the presence of a transient liquid phase, which accelerates plasticity, grain boundary/surface diffusion and mass transport. Several ULES techniques have been developed in the past 50 years, and a common feature of all of them is low temperature consolidation, through mechanisms not yet fully understood, enabling multi-material integration (e.g. organics and inorganics). This research could transform the traditional firing of functional and structural materials. Early stage work on ULES, started in the 1960s, clearly demonstrated cohesion between the compacted particles exceeding what was possible if simply produced by Van der Waals bonding, suggesting the formation of primary inter-particle bonds. Surprisingly, metals Cold Sintered (CS) in dry conditions at room temperature can be even stronger than their counterparts sintered at high temperatures (typically $\approx 2/3 T_m$). Hydrothermal Hot Pressing (HHP) was originally conceived in the context of sustainability and environmental preservation, with some examples being the concept of 'synthetic rock' for immobilisation of toxic/radioactive waste and the consolidation of high surface area porous ceramics for filtration. Follow up work on HHP considered the possibility of recreating in the lab bio-mineralisation using hydroxyapatite and bioglass (including hybrids) as proof of concept. Recent work on the Cold Sintering Process has demonstrated the potential to bridge the processing gap of multi-material devices (sensors, batteries, 5G antennas, electronic components and biomaterials), enabling integration of polymers, ceramics and metals without degradation of the individual components both at the bulk and interface level. The absence of heating unlocks grain boundary design to an unprecedented level, offering further degrees of freedom in tuning functional properties.

This review provides a wide perspective on room temperature consolidation, and covers the related but fragmented work published (≈ 450 papers) during the past 50 years, encompassing the relevant work developed in different disciplines including chemistry, physics, biology and geoscience. Liquid-assisted or liquid-mediated phenomena involving diffusion, plasticity, rheology, and grain growth are still largely unexplored in material science. The purpose of bringing together this literature is to build a general and multidisciplinary knowledge to guide future research directions. Both the reduction of energy consumption and carbon footprint are driving the growing interest in ULES, which could reinvent the concept of sintering, 'rendering kilns obsolete'. Also, ULES has the potential to produce new classes of materials that cannot be fabricated using conventional routes.

ARTICLE HISTORY

Received 12 September 2019
Revised 12 December 2019
Accepted 16 December 2019



KEYWORDS

Ultra Low Energy Sintering (ULES); Hydrothermal Hot Pressing (HHP); reactive Hydrothermal Liquid Phase Sintering (rHLPS); Hydrothermal Reaction Sintering (HRS); Cold Sintering (CS); Cold Sintering Process (CSP)

1. Introduction

Most ceramics are prepared using green forming followed by firing, which is a highly energy intensive process involving temperatures usually above 1000 °C. Because of this, ceramics have higher embodied energy (energy dissipated to create 1 kg of usable material, see figure 4.19 in Ref [1]) compared to polymers or metals. The firing of construction bricks is currently

responsible for ≈ 41 teragrams of CO₂ emissions into the atmosphere per annum [2]. Most of the energy used for heating is irreversibly dissipated through the furnace insulation and lost during cooling. Since sintering is a process driven by reduction of surface energy, a possible way to reduce energy consumption might involve selective heating of the surface of the particles. This approach, idealised in electromagnetic assisted processing techniques (e.g. microwave and spark

CONTACT Salvatore Grasso  s.grasso@swjtu.edu.cn  Key Laboratory of Advanced technologies of Materials, Ministry of Education, School of Materials Science and Engineering, Southwest Jiaotong University, Chengdu 610031, People's Republic of China

© 2020 The Author(s). Published by Informa UK Limited, trading as Taylor & Francis Group

This is an Open Access article distributed under the terms of the Creative Commons Attribution License (<http://creativecommons.org/licenses/by/4.0/>), which permits unrestricted use, distribution, and reproduction in any medium, provided the original work is properly cited.

plasma sintering), has not proven realistic. The idea of promoting atomic diffusion at a particle's surface without providing additional heat, is possible in the presence of a liquid, typically water, that is capable of dissolving/interacting and promoting mass transport between the sintering particles.

By lowering the sintering temperature to near room temperature ($<300\text{ }^{\circ}\text{C}$), the embodied energies for conventionally hot fired ceramics in the case of industrial production, range between 40 (alumina) and 200 MJ kg^{-1} (boron carbide) [1], are expected to be lowered by at least one order of magnitude. Sohrabi [3] on the lab scale calculated that the energy consumed in the consolidation of BaTiO_3 powder can be lowered by two orders of magnitude from 2800 to 30 MJ kg^{-1} using the Cold Sintering Process (CSP). Energy calculations, done at lab scale level by researchers at the University of Sheffield, suggest that the consolidation of 1 kg of ZnO requires 291 MJ kg^{-1} based on hot-firing, equivalent to a climate change impact of 42.5 kg CO_2 . On the other hand, cold sintering requires only 162 MJ kg^{-1} , resulting in a carbon footprint of 23.6 kg CO_2 [4].

Taking inspiration from inorganic materials produced in nature, there are plenty of everyday examples of inorganic materials formed at room temperature without the need of additional heat. These include sedimentary rocks produced by lithification (literally, the process of turning particles into stone), stalactites from precipitation of minerals

from mineralised water dripping through cave ceilings, bones/teeth from bio-mineralisation, construction of buildings from cementation and spicules (sea sponges) from the polycondensation of silicic acid. For several centuries scientists have tried to emulate these processes. Research is still not sufficiently advanced to replicate hierarchical structures as in nature; the difficulties are related either to the lengthy timescales involved – the lithification process can take several thousands of years – or because of the inherent complexity in bio-chemical systems.

Several consolidation techniques for compaction of powders at near room temperature have been proposed. This review covers the complexity of phenomena occurring under Ultra Low Energy Sintering (ULES) conditions, bringing together highly multidisciplinary aspects of natural science and material science, including chemical weathering/geology, thermodynamics of liquids solutions, metallurgy/plasticity, hydrothermal crystal growth and biomineralisation as illustrated in Figure 1.

This review embraces the fragmented relevant literature published in the past 50 years and provides a general knowledge-base on ULES. Our ambitions are: (i) to capture the originality of early work (starting from the 1960s) in order to substantiate more recent publications; (ii) define guidelines to describe the consolidation mechanisms by linking together knowledge well-established in different fields; (iii)

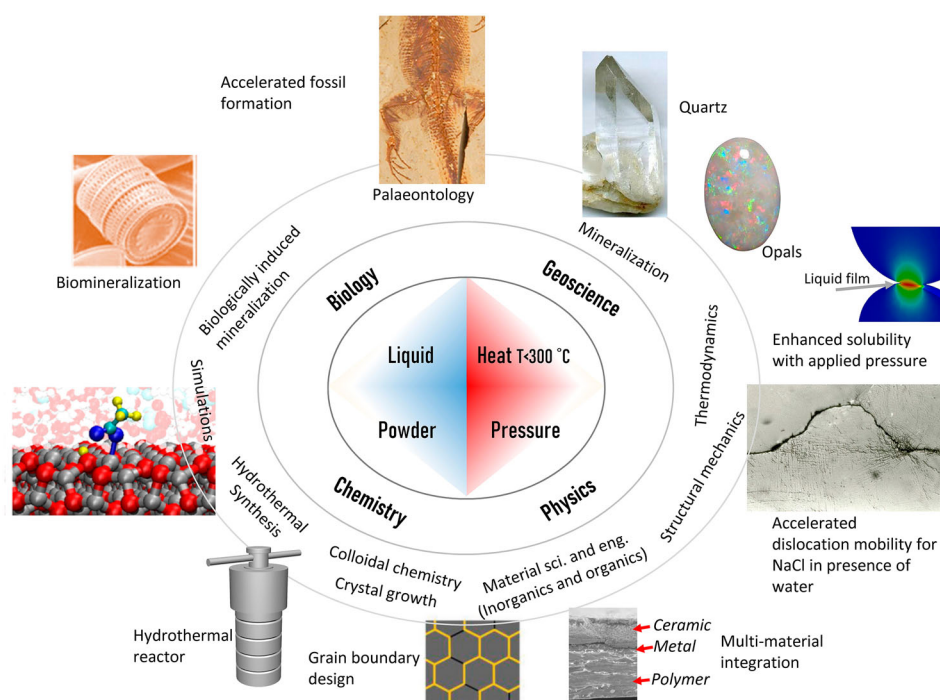


Figure 1. Branches of science underpinning ULES. The combination of four components: liquid, powder, heat and pressure, requires a multi-disciplinary approach covering physics, chemistry, geoscience and biology. A synergistic knowledge-base, built up from a wide range of disciplines, ranging from material science and engineering to palaeontology [5], could aid the understanding of these techniques to support their technological and scientific impact.

predict a processing window (i.e. pressure, type and amount of liquid, setups and temperature) for different materials based on their ionic, metallic or covalent bonding.

1.2 Historical perspective

Going back to early civilisation, we can easily imagine that our ancestors might have squeezed in their palms some wet soil trying to make it stronger or harder. A similar situation might arise when a child instinctively tries to put back together a broken toy.

Isaac Newton was the first to suggest that two particles brought into close contact would adhere, ‘two polish’d marbles by immediate contact stick together’ [6]. The possibility of compacting particles together has a more recent history. Between 1800 and 1820, William Hyde Wollaston was the first to recognise particle bonding [6] by compacting platinum mud (and later other rare metals) to produce dense and strong wires. Platinum is a high melting point material (1768 °C), and at that time it was difficult to draw it into wires using ordinary melting and casting techniques. Wollaston, who was a chemist, prepared particles of platinum, and then produced a mixture of these particles dispersed in water (‘platinum mud’). In order to make a dense block he developed a press, shown in Figure 2, composed of a hollow brass die into which he fitted a \approx 25 mm diameter piston. Applying a weight of 30 tonnes to the ram, equivalent to a pressure of the order of 500 MPa, increased the packing density from 20% to nearly 50%. The result was a pellet that was ‘hard and

firm’. After heating in a Staffordshire coke furnace and forging, a 99% dense material suitable for making platinum wire with the ‘highest tenacity’ was produced. The work by Wollaston is often recalled in the early literature on Van der Waals interactions, however, metallic bonds could have formed during pressing as described in section 3.1.1.

In 1964, Brill and Melczynski [8] from the Fritz-Haber-Institut in Germany, in a paper entitled ‘Hydrothermal Sintering’, proposed a low temperature (< 100 °C) consolidation method for metal powders. They reported

We found that the iron particles always cake together if they are placed in close contact with one another and then treated with warm water or boiled with water. The hydrothermally sintered solids are strong enough to be turned on a lathe; the exposed surface acquires the typical appearance of iron.

Similar effects were also observed for aluminium and zinc, as metallic particles were joined together in the form of Boehmite and ZnO, however, these products were not strong enough for any structural application. An advantage clearly recognised already at that time was the potential for integration with non-metallic materials such as paper and plastics [8].

In 1964, Turba and Rump [9,10], using the setup shown in Figure 2(c), investigated the mechanism of cohesion in BaSO₄ powders compacted both in dry as well as moisturised conditions. For dry-pressed BaSO₄, they concluded that Van der Waals forces were the most significant particle-particle interactions. Under wet conditions, other effects should be taken

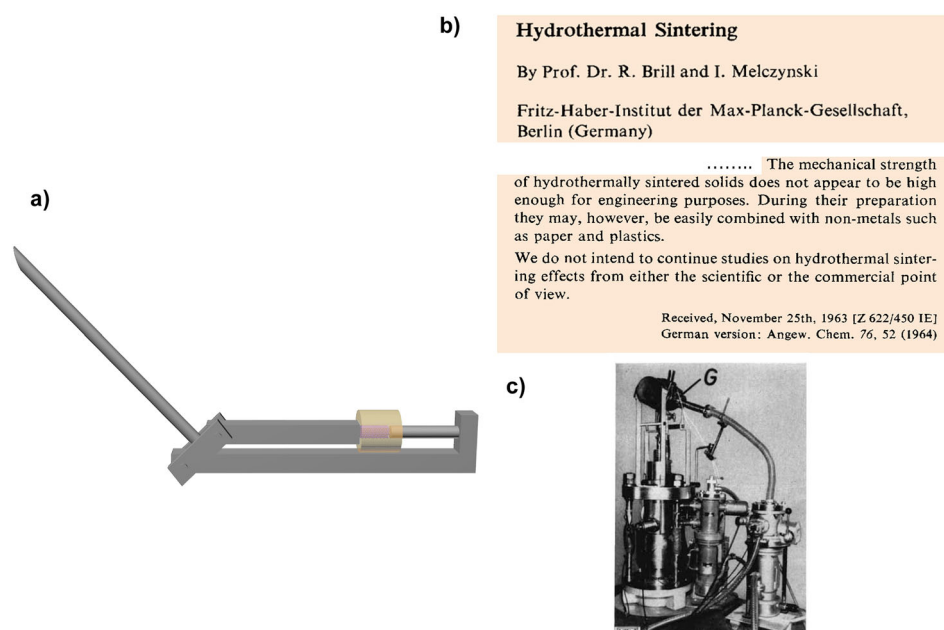


Figure 2. (a) Wollaston Press developed in 1829 for compaction of loose platinum mud into a firm pellet [7]. (b) Extract from early work by Brill and Melczynski dated 1964 [8] on hydrothermal sintering. At the time, the authors did not intend to continue studies because they could not find any useful application. (c) Setup developed by Turba and Rump [9] for carrying out ‘cold sintering’ experiments: a systematic correlation between strength of barite pellets and amount of water was found.

into account, such as local fusion phenomena, solvent actions and chemical reactions. In their analysis, they focused on a fundamental aspect of ULES, inter-particle bonding formation; the measured adhesion after wet compaction was significantly larger than the Van Der Waals interaction for dry-pressed BaSO_4 . They concluded that the increased cohesion strength might have been due to the presence of water that might have induced particle cohesion/bonding under the compacting pressure. The idea to precisely measure the amount of absorbed water, and not to assume that a powder stored in air is 'dry', should be accepted as a common practise in the modern literature.

2. Recent developments in near room temperature consolidation: processes and methods

To gain a full perspective on ULES, it is essential to analyse the rather fragmented relevant literature. This review aims to build a shared knowledge common to all ULES techniques covering organic (polymers and biological) and inorganic compounds (ceramic, salts and metals) where their upper processing temperature limit is 300°C . Both ULES in wet and dry conditions are discussed as the techniques might share common consolidation mechanisms related to the application of high pressure ($>300\text{ MPa}$) or the combination of pressure and presence of a liquid. Typically, ULES of metals and polymers is done in dry conditions (see Section 2.2) while other materials are processed in wet conditions by adding a liquid (see Section 2.3)

2.1 Overview of ULES processes

This section presents the most significant developments and summarises the milestones, as presented in Figure 3. Chronologically, the techniques appear in the following order: Hydrothermal Reaction Sintering (HRS) in 1976 [11]; Cold Sintering (CS) in 1979 [12]; Hydrothermal Hot Pressing (HHP) in 1984 [75]; reactive Hydrothermal Liquid-Phase Densification (rHLPS) in 2007 [76] and CSP in 2016 [77].

The differentiation between the sintering techniques is clearly presented in Table 1. The Salient features of each technique are schematically presented in Figure 4. The aim of this clear differentiation is to define direct correlations between the processing parameters and microstructures and properties of the materials produced by these techniques. The number of publications on ULES per year is given in Figure 5.

Hydrothermal Reaction Sintering (HRS) [11,82] employs as a starting material a metallic pre-compacted powder that is oxidised by a supercritical water solvent heated within a millimetre-sized metal sealed capsule (made of platinum which is permeable to generated hydrogen) where the self-generated

pressure can reach 100 MPa with a temperature approaching 1000°C (which is well above the 300°C discussed above, but still well below the traditional consolidation temperatures). To date, 16 papers (22 including literature in the Japanese language) have been published on HRS. Owing to the complex experimental setup and very small size of the samples, the technique has not found any applications. HRS might be reconsidered in the future as sintering techniques employing supercritical water are expected to be developed.

A more versatile approach to consolidate ceramic powders named HHP was proposed by Yamasaki in 1984 [29]; published first in Japanese and two years later in English. To date 207 articles have been published on HHP, indicating a well-developed scientific literature on the topic. Most of the work on HHP, 170 papers in total, has been published by Japanese groups, with 57 papers by Yamasaki Nakamichi's and 42 by Yanagisawa Kazumichi's groups. The HHP literature is diverse and well worth examining. There are several links to sustainable processing of ceramics inspired by geological rock formation and bio mineralisation. The initial research on HHP was mostly driven by the need for encapsulation of radioactive waste by the development of bio-inspired processing routes. In HHP, the sintering environment replicates hydrothermal processing conditions because the environment is sealed, unlike in CSP where the processing vessel is not completely sealed to allow evaporation of the liquid phase. The hydrothermal processing environment has an effect on both the crystal growth and the densification kinetics.

rHLPS was patented in 2012 by Riman et al. [76]. Follow up work on BaTiO_3 was published by Vakifahmetoglu et al. in 2016 [83]. The experimental setup is shown in Figure 4, in which a partially sintered (porous) material undergoes a chemical reaction (e.g. $\text{Ba}(\text{OH})_2 + \text{TiO}_2 = \text{BaTiO}_3 + \text{H}_2\text{O}$) while immersed in a liquid under hydrothermal conditions ($T < 200^\circ\text{C}$, up to several days). Only a few works have focused on this method, mostly because of the lengthy processing times and difficulty in reaching a complete reaction.

While the trends in the number of publications on HHP and CS have been rather discontinuous over the past 4 decades, interest in CSP has recently experienced a very rapid growth. Since 2016, 92 papers have been published on the CSP –, with Professor Randal's group publishing most of 77 of them [77], – with the number of publications expected to grow exponentially over the next couple of years.

2.2 Cold Sintering in dry condition: materials and applications

Cold compaction of KBr and other halide salts is a common practice for producing optically transparent

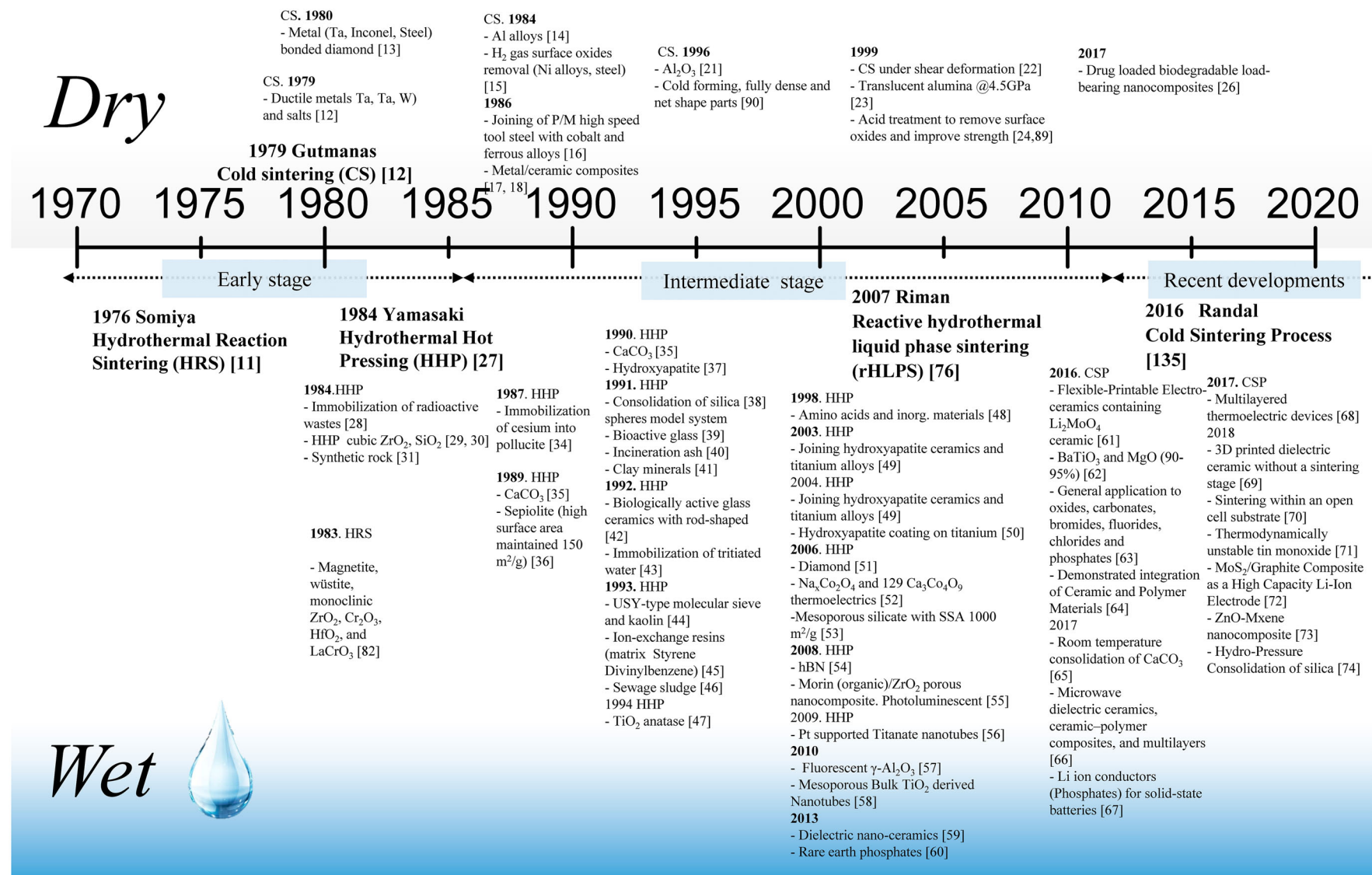


Figure 3. Road map tracing milestones in near room temperature consolidation ($T < 300\text{ }^{\circ}\text{C}$) over the past four decades. Several techniques have been developed, based on dry (top) and wet (bottom) ULES [11–74].

Table 1. Comparative analysis of ULES techniques.

	Gutmans' Group, 1979, Cold Sintering, CS [12], Israel	Yamasaki's Group 1984, Hydrothermal Hot Pressing, HHP [27,75], Japan	Riman's Group, 2007, reactive Hydrothermal Liquid-Phase Sintering, rHLPS [76], USA	Randall's group, 2016 Cold Sintering or Cold Sintering Process (CSP) [77], USA
Key features	No heating and uniaxial pressure (Figure 4(a))	Hydrothermal conditions and uniaxial pressure Figure 4(c)	Hydrothermal reactive sintering (no uniaxial external pressure), Figure 4(d). Sample pre-compaction/firing is needed prior to rHLPS.	Heating and uniaxial pressure (not hydrothermal) Figure 4(b)
Pressure	0.5 to 4 GPa	<300 MPa	Hydrothermal	<1 GPa
Temperature	Room temperature + annealing	<350 °C	<250 °C	<250–300 °C above the boiling point of the liquid
Pressing time	15 s, 1 min sintering + extraction (whole cycle, pressing and extraction)	10–60 mins dwelling time	<70 h hydrothermal reaction time	<60 min
Dies design	Piston-cylinder apparatus from sintered carbides. Figure 4(a)	Consolidation under uniaxial pressure and within a hydrothermal sealed chamber. Figure 4(c)	Cold pressing + hydrothermal reactions. Figure 4(d)	Piston-cylinder die. Figure 4(b)
Sample diameter	Diameter 5–20 mm	10–30 mm	10–30 mm	5–15 mm
Hydrothermal conditions (Y/N), presence of liquid	Done in dry conditions	Yes, hydrothermal reactor chamber (acidic or caustic solutions)	Yes, reactive solvent to produce a desired compound	No, acidic or caustic solutions and organic solvents
Pressure built up between solid (particle) and liquid during sintering (capillarity excluded).	NA	Hydrothermal pressure	Hydrothermal pressure	No pressure between liquid and solid, liquid is free to escape if porosity is open. Inter-particles liquid film might be instead subjected to pressure.
Second phases employed	Diamond	Resin [45], biomaterials, radioactive waste, metal ceramic composites	Not attempted	<ul style="list-style-type: none"> • Wide range of polymers • 2D materials and nanomaterials
Materials	Metals including refractory metals, inorganics as NaCl, CdTe, RbI	Oxides, carbonates, bromides, fluorides, chlorides and phosphates see	Oxides, carbonates, fluorides, chlorides and phosphates.	Oxides, carbonates, bromides, fluorides, chlorides and phosphates their composites
Remark	Not applicable to brittle materials	Some materials might require further heat treatment to complete consolidation and/or remove excess of water		The evaporation step is included in the processing as the sintering chamber is not sealed
Sintering mechanism	Plastic deformation of ductile particles	Transient liquid phase sintering		Transient liquid phase sintering, plastic deformation or surface/grain boundary diffusion activated by the liquid reaction with the powder
Final density	Close to theoretical	70–98%, full density achieved with a post treatment	70–90%	80–100%
Typical Advantages	Avoids grain growth or thermal degradation in metastable and nanostructured materials [78]	<ul style="list-style-type: none"> • Low temperature sintering for better replication of bio-mineralisation • Low temperature nuclear waste encapsulation • Recycling of waste into artificial rocks [79] • Crystallisation accelerated by hydrothermal conditions [80] 		<ul style="list-style-type: none"> • Single step for sintering consolidation near to full density • Integration of Ceramics with polymers [81] • improved functional properties • possible integration in 3d printing

Note: Key features, thermodynamic processing parameters and composition are taken into account. Sealing of sintering chamber, presence of a liquid, processing under hydrothermal or atmospheric conditions are the main distinctive features.

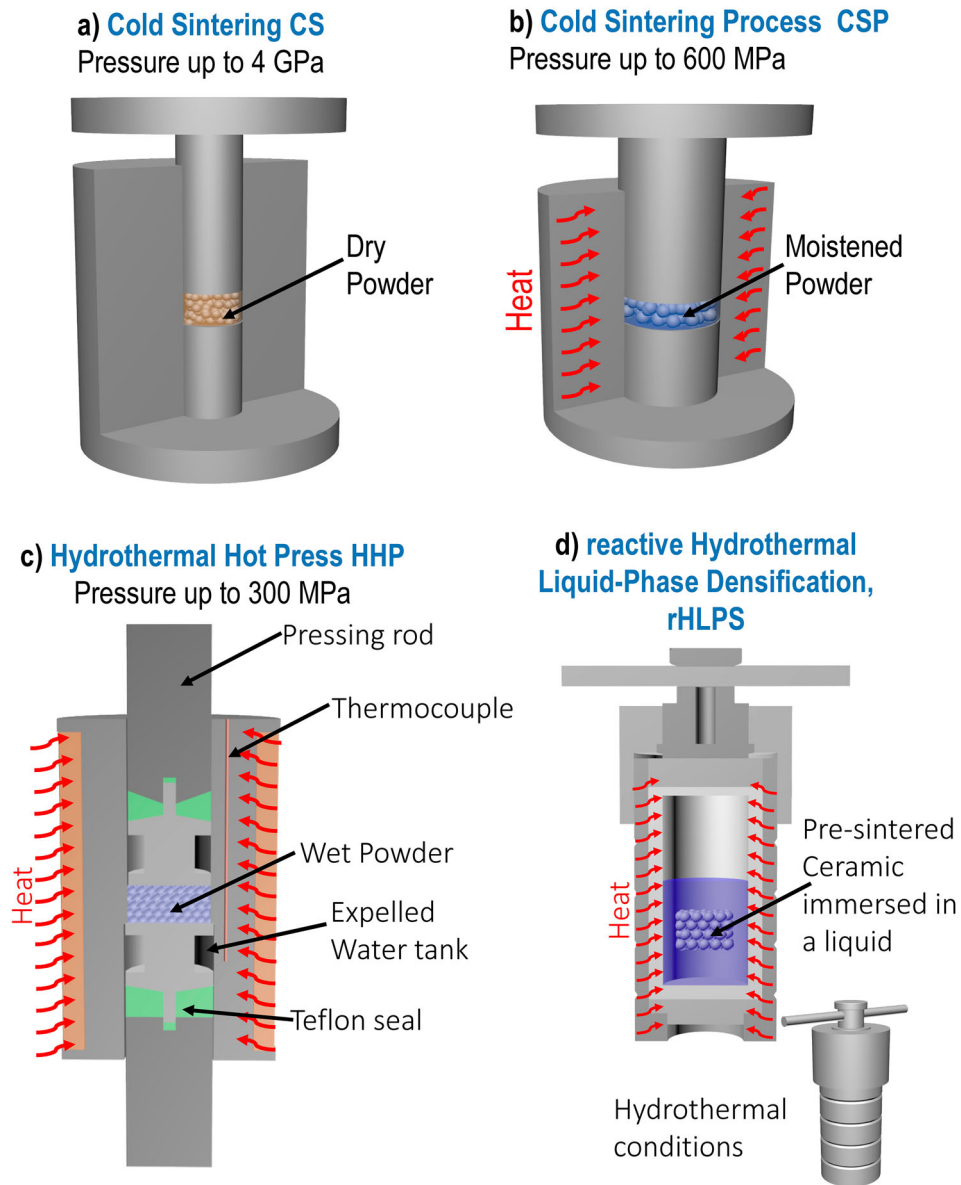


Figure 4. Experimental setups used for ULES. The main differences are presented in Table 1. (a) CS, (b) CSP, (c) HHP, and (d), rHLPS.

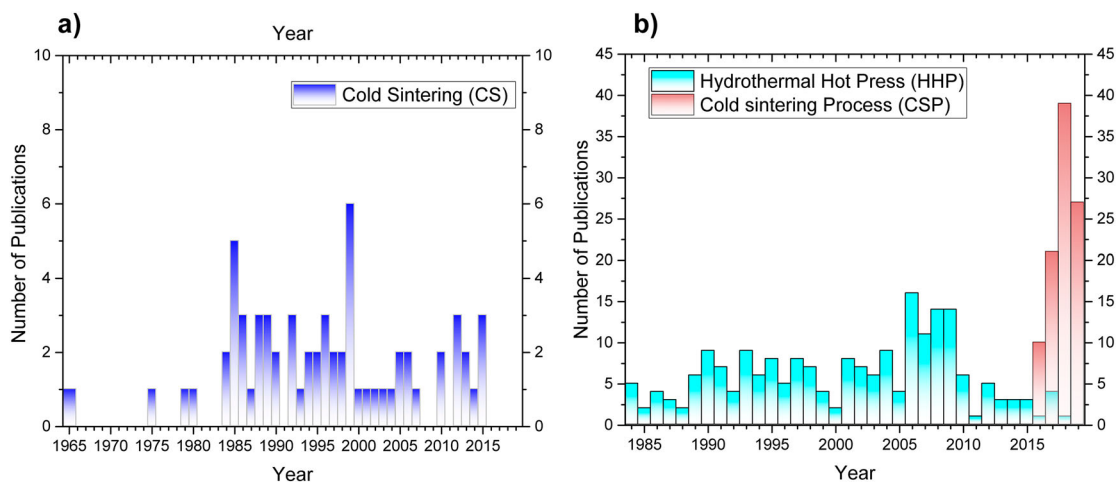


Figure 5. Number of publications on ULES per year, as of June 2019: (a) in dry conditions using CS; (b) in the presence of a liquid using HHP and CSP.

samples for infrared spectroscopy. The materials to be investigated are mixed with a transparent solid matrix (typically KBr). Starting from 1952, Schiedt and Reinwein [84] along with Stimson and O'Donnell [85] employed cold compaction for preparing samples of KBr or alternatively CsI, KCl, AgCl samples for infrared spectroscopy. Powders were pressed in evacuable pellet press dies. Vacuuming prior to pressing allows removal of occluded air, which avoids cracking of samples. Mirror polished pressing punches allow the samples to be optically transparent and suitable for infrared spectroscopy without further preparation. However, such work was motivated to produce samples for infrared spectroscopy rather than research on ULES.

Coming back to dry consolidations routes, CS has been used to consolidate ductile metallic powders. Professor Gutmanas' group from Israel published 22 papers on 'cold sintering' starting from 1979 [12], with 10 papers from Balkan countries, 7 from China and 5 from Brazil.

The early work on room temperature compaction [12] of metallic powders was initiated in 1979 by Gutmanas' group. It involved the densification of 'ductile powders' like Al, Cu, Co, Fe, and Fe-Ti alloys (316L, Inconel 600 and Ti6AlV) and refractory metals such as Nb, Mo, Ta and W. The consolidation was possible under a plastic deformation regime as discussed in Section 3. Ionic salts like RbI were also consolidated using CS. However, other brittle materials, including InSb, NaCl, TiC, WC and MgO, could not be densified, which was attributed to their limited plasticity and high yield stress at room temperature. The idea to use high pressure to promote bonding was also applied in 1986 in the CS of ferrous powders [86] and metal matrix composites containing reinforcing ceramics (CrO₂ [17], VC [87], and WC [88]).

Another good example of the use of CS is the production of diamond composites metal matrix cutting tools [13]. The room temperature processing avoided any diamond graphitisation, and a post heat treatment allowed the formation of interfacial carbides, which contributed to an improved interfacial strength. Good evidence of the relationship between particle surface condition and inter-particle adhesion was demonstrated by hydrogen treatment, which induced chemical reduction of the powder particles, contributing to a pronounced increase in the rupture strength [15]. Analogously, a clear demonstration of the benefit of surface cleaning on CS was shown by Lashmore et al. [24] and Dariel et al. [89]. Their work suggests that acidic washing of the starting silver powders was sufficient to remove surface oxides, thus allowing a self-soldering effect of silver during CS.

Follow-up studies attempted consolidation of ZrO₂, α -Al₂O₃ [19] and γ -Al₂O₃ [23] by employing pressures even higher than 4 GPa, with densities exceeding 90% achieved in the case of zirconia because of its pressure

induced phase transformation. Extensive work on high pressure sintering of ceramics was done by Augusto Neto in his master's thesis back in 1990 [19]. Alumina powder compacted under such high pressure at room temperature reached a relative density of 85–90%, but its hardness was ten times lower than conventionally sintered ceramics. This was not due to residual porosity, but probably to the limited adhesion between the particles.

Starting from 1996, CS has been proposed as a mass production technique for consolidation of net-shaped parts made of aluminium/copper, copper coated tungsten and nickel/aluminium [90]. Agatonovic et al. [22] combined uniaxial pressure with rotation of the pressing piston up to an angular displacement of 1000° for consolidation of molybdenum powders. Compared to materials consolidated in dry conditions, materials processed in the presence of an acid had a 5-fold increase in rupture strength. Recent work has been reported by Gutmanas et al. [26] on drug loaded biodegradable scaffolds for bone ingrowth produced using CS. The use of room temperature processing allowed the integration of dissimilar materials, while another advantage was the incorporation of drugs (antibiotics and anticancer) for enhancing the biological properties of the scaffolds.

2.3 Key features of liquid-assisted ultra low energy sintering: materials and applications

2.3.1 Early stage

Early work on ULES in the presence of a liquid phase dates back to 1973 when Roy et al. [91] prepared very high compressive strength cements (\approx 700 MPa) by pressing them at 250 °C under a pressure of 345 MPa. A small amount of water was added to anhydrous cement resulting in a final degree of hydration of about 30% (well below fully hydrated as in the case of casting). The 5-fold improvement in compressive strength was related to the reduced porosity of samples compacted under an applied pressure.

In 1976, Hirano and Somiya [11] at the Tokyo Institute of Technology developed the HRS approach for making dense materials starting from a metallic pre-compacted powder under hydrothermal treatment in an airtight Pt capsule permeable to H₂ at 850 °C for 1–3 h. The high temperature reaction between the metal powder and H₂O allowed the formation of the oxide, with a concomitant release of H₂ through the permeable membrane (capsule size: 2.7 mm in internal diameter 0.15 mm thick, and 35 mm long). Materials processed by this technique include ZrO₂, Al₂O₃, HfO₂ [82], Al₂O₃–ZrO₂, iron oxides [92], Cr₂O₃ [11] and LaCrO₃. The sintering temperatures were typically lowered by 300–500 °C compared to conventional sintering temperatures. A limitation of the technique is the high cost of the Pt capsule.

2.3.2 Hydrothermal hot pressing

According to Yamasaki et al. [75] 'The hydrothermal hot-pressing method has two characteristics: continuous compression of samples under hydrothermal conditions and space for water retreat'. The combination of these two features clearly represents a novel processing technique. Initial work on HHP was reported in 1986 (1984 in Japanese language). The work has been applied to many materials (see Figure 7 below). It is worth highlighting that the solubility and reactivity of many inorganic compounds increases under hydrothermal conditions [93].

Wide range of materials. Several crystalline and amorphous materials [75] have been consolidated by HHP at 350 °C, including SiO₂ [31], ZrO₂, TiO₂ [94], CaCO₃, Ca(OH)₂, Al(OH)₃, plastics, cement, etc. Even translucent cubic zirconia [95] was prepared from a co-precipitated gel by hydrothermal hot-pressing at 350 °C and subsequent sintering at 1350 °C. Consolidation and crystallisation of amorphous titania by hydrothermal hot-pressing with a Vickers hardness 7.83 GPa was achieved at 350 °C (slightly above the typical temperature limit for ULES) under 200 MPa by Yanagisawa et al. [47]. In 2006, Yokosawa et al. [51] attempted HHP of diamond powder in the presence of a chlorinated hydrocarbon under a pressure of 1 GPa (their equipment was particularly advanced and was able to apply pressure up to 5 GPa). Raman spectroscopy of the sintered material detected only sp³ bonds, suggesting the formation of diamond to diamond bonding.

Silica and its allotropes are some of the most studied materials processed by HHP. Low-temperature hydrothermal sintering of dense nanometric α -quartz suggests that water played a key role [96,97]. Costa et al. [98] identified, using Raman spectroscopy, an accelerated condensation reaction of silanol groups in the presence of water.

The applications of HHP are well widespread and range from thermoelectrics to biomaterials. For example, Katsuyama et al. consolidated Na_xCo₂O₄ [52] and Ca₃Co₄O₉ [99] thermoelectrics using HHP, and they reported an increase in the power factor induced by preferred crystallographic orientation promoted by the uniaxial pressure. The hydrothermal hot-pressing method [60] was proposed to avoid thermal decomposition of rare earth phosphates, which are susceptible to thermal decomposition. Samples of lanthanum and yttrium ortho- and poly-phosphates LaPO₄, La(PO₃)₃ [100], YPO₄, Y(PO₃)₃ were fabricated using HHP.

The below HHP work is grouped with respect to their applications.

Nuclear encapsulation, high surface area and filtration. Initial work on HHP was driven by the

need to develop sintering techniques with reduced sintering temperatures for the immobilisation of radioactive waste [31] containing caesium. Silica was chosen as the immobilising material, and the process was likened to 'lithification' [31]. Here, particular attention was devoted to the strength and leaching resistance of the sintered materials, as the matrix encapsulating radioactive waste is required to have a long service life. Immobilisation of tritiated water (an undesired by product from nuclear reactors) using hydrothermal hot-pressing [101] was also adopted, allowing the development of materials with excellent leaching resistance. Ion-exchange resins [45] were also consolidated by HHP with the aim of reducing the volume of the radioactive waste. The recurring concept of synthetic rock was employed to produce artificial pollucite (a zeolite mineral (Cs,Na)₂Al₂Si₄O₁₂·2H₂O used for Cs encapsulation) [102] and for consolidation of sepiolite (Mg₄Si₆O₁₅(OH)₂·6H₂O) while maintaining its high surface area exceeding 150 m² g⁻¹ [103].

Preparation of molecular sieves by HHP was proposed by Meng et al. [44]. Zeolite derived from fly ash (ZFA) prepared by HHP was applied to ammonium removal from sea water [104]. By optimising the processing conditions, Nakahira et al. [105] were able to maintain the large surface area – of over 700 m² g⁻¹ – of the starting Y-zeolite powder in the fabricated HHP compacts. HHP is also capable of consolidating bulky mesoporous silica achieving a dense microstructure free from large voids while maintaining a high value of specific surface area exceeding 1000 m² g⁻¹ [106]. Bulky mesoporous silica Pd-MCM-41 (palladium catalyst supported on mesoporous catalyst) processed by HHP resulted in a high surface area of over 1000 m² g⁻¹ [107]. In a follow-up work by Kubo et al. [56], Pt-supported titanate nanotubes and their photocatalytic properties were investigated.

Waste valorisation and recycling. Alkali-activated incinerator ashes [108] are currently becoming an environmental friendly alternative to cement and bricks. Recycling technologies around HHP were reviewed by Yamasaki Nakamichi [109] in 2005. Sludge ash, which is a by-product of waste water treatment [110], ashes from incinerators [111], waste glasses [112], steelmaking slag [113], and blast furnace slag [114] were consolidated by HHP, suggesting a viable recycling and valorisation route for these materials. In 2008, reuse of glass from cathode-ray tube TVs by HHP was proposed by Matamoros-Veloza et al. [115]. Their approach was to apply HHP to finely ground powder followed by foaming at 600 °C, resulting in a low thermal conductivity of 0.21 W (m K)⁻¹. More recently, in 2005 Xue et al. [116] and later on Song et al. [117], employed HHP (45 min and 7 MPa at 200 °C) as a sustainable method for immobilising

heavy metal ions, with a good fixation effect on metals such as Cu, Zn, Cd and Pb within an inert matrix derived from fly ash. Using waste glass from TV screens, preparation of porous glass with low thermal conductivity (0.2 W (m K)^{-1}) [118] was achieved by HHP followed by foaming (induced by entrapped water) at 750°C for 1 h. A similar approach was also applied to other systems resulting in a final density as low as 0.40 g cm^{-3} obtained for SiO_2 (α -cristobalite and quartz) and CaSiO_3 (wollastonite) [119].

Bio-related. Because of its mild processing conditions, HHP is clearly a consolidation technique closer to biomineralisation compared to conventional sintering (see Figure 1). Translucent hydroxyapatite ceramics were produced using HHP (300°C , 50 MPa) starting from amorphous calcium phosphate [103].

Bioactive glasses in the Na_2O – CaO – SiO_2 – P_2O_5 system [39] processed by HHP at 350°C under 50 MPa were almost pore free, consisting of homogeneously precipitated rod-shaped crystals of $\text{NaCa}_2\text{HSi}_3\text{O}_9$ and $\text{Na}_2\text{Ca}_2\text{Si}_3\text{O}_9$ with length $\sim 3 \mu\text{m}$ and width $\sim 0.3 \mu\text{m}$. The Vickers hardness and the compressive strength of the glass-ceramics were 3 GPa and 460 MPa, respectively. The fracture toughness increased by a factor of 5 up to $2.5 \pm 0.3 \text{ MPa m}^{1/2}$ compared to that of bioglass prepared using conventional sintering. Gamoh and Yamasaki [48] exploited the HHP conditions for enhancing polymerisation of amino acids while consolidating inorganic materials, making HHP (270°C , 60 MPa) an ideal technique for integration of inorganic/organic materials. [120]

Similar to the joining under dry conditions mentioned in Section 2.2, hydroxyapatite (HA) and titanium (Ti) were bonded by HHP [49], with a HA coating sintered and adhered to a titanium (Ti) rod using HHP at 135°C under 40 MPa [121]. The in-situ formation of hydroxyapatite-whisker ceramics during HHP (300°C , 40 MPa) was demonstrated by Li et al. [122], with an enhancement of bending strength up to 56 MPa achieved in the presence of an ammonia solution, which promoted the growth of the elongated crystals. HHP made possible the consolidation of hydroxyapatite loaded with adipic acid intercalated complexes, which had better biocompatibility compared to unloaded ones [123]. Onoki et al. [124] prepared apatite chitosan polymer composites at 150°C for 2 h at 40 MPa; their investigation suggests that HHP allows a fine mixture (submicrometre scale) not achievable with other techniques. Irie et al. used HHP (50°C , 2 MPa) to fabricate DNA/polycation complexes for clinical treatments requiring thin membranes or films, such as protective membranes for stomatitis and incised oral wounds [125].

Integration of organics, inorganics and thermally fragile materials. Examples of organic–inorganic

integration clearly highlight the merits of HHP in suppressing thermal degradation of the consolidating constituents, and this opens up the possibility of creative innovations and unexplored applications. The reinforcement of chitosan (a sugar) with xonotlite (calcium silicate hydrate) fibres [126] and calcium silicate compacts with rice husk were achieved using HHP (150°C , 20 MPa) by Udawatte et al. [127]. Likewise, Sun et al. [128] employed short polyvinyl alcohol (PVA) fibres to improve the mechanical properties of brittle fly ash samples, with the constituents solidified using HHP (150°C , 20 MPa). This promoted a transition from brittle to ductile behaviour, with a 6-fold increase in the strain to failure for samples loaded with 1 wt-% of fibres. ZrO_2 /morin [55] and $\gamma\text{-Al}_2\text{O}_3$ [129] /fluorescein (morin and fluorescein are natural and synthetic molecules used as dyes, respectively) composites were prepared using HHP (200°C , 90 MPa) by Liu et al. In the latter, the photoluminescence of the fluorescein within the porous nano solid was enhanced as compared to pure fluorescein. This was attributed to the local interaction of the organic molecule with the surface atoms of the $\gamma\text{-Al}_2\text{O}_3$ pores.

Xie et al. sintered to full density a new $\text{Sn}_{1.24}\text{Ti}_{1.94}\text{O}_{3.66}(\text{OH})_{1.50}\text{F}_{1.42}$ phase with a decomposition temperature of only 300°C , which could only be densified by HHP [130] (at 270°C and 80 MPa for 4 h). Interestingly the colour of the final material could be tuned from yellow to reddish-brown by increasing the amount of water. Dense compacts of titanate nanotubes ($\text{H}_2\text{Ti}_n\text{O}_{2n+1}$) were prepared by HHP (200°C , 40 MPa) [131]. Because of the mild processing conditions, the resulting materials had dense microstructures, and their high BET surface areas and tubular nanostructure were maintained.

2.3.3 Reactive hydrothermal liquid phase sintering

Several compositions have been processed by rHLPS [76] at 240°C including BaTiO_3 , SrTiO_3 , $\text{Ba}_{0.5}\text{Sr}_{0.5}\text{TiO}_3$, $\text{Pb}(\text{Zr,Ti})\text{O}_3$, CoFeO , NiMoO and others. Work on this technique has been rather limited because of the slow reaction kinetics, for example 72 h was needed to produce a 90% dense BaTiO_3 [83]. Since the process involves the use of pressure, comparative analysis between rHLPS and HHP could help to decouple the effects of chemical reactions from consolidation; this could pave the way for hybrid techniques where the compacting uniaxial pressure is for example applied after a hydrothermal reaction reaches completion.

2.3.4 Pressure-less wet ULES and 3D shaping

Professor Jantunen's group at the University of Oulu, Finland has carried out related but different research from CSP and other pressure-assisted sintering techniques. They widely employed water-soluble lithium molybdate and processed at room temperature (drying is done in a subsequent step and not while pressing as

in CSP) in the absence of uniaxial pressure. By using water and water-soluble Li_2MoO_4 powder, 3D printed dielectric ceramics can be produced without heating under pressure-less conditions [69]. Moreover, electro-ceramic composites constituted by barium strontium titanate and lithium molybdate were consolidated at room temperature [132]. Their work [133] aimed at increasing the bulk density by reducing the amount of water entrapped in the material, suggesting that improved dielectric properties could be achieved when using coarse particles. Coming back to net shape manufacturing, the only other example of 3D shaping and ULES in the literature was reported by Jiang [134] et al. for silica using isostatic pressing (300 MPa at room temperature) and a shaped rubber mould.

2.3.5 Cold sintering process (Randall's method)

The CSP was developed at Pennsylvania State University by Prof Clive Randall along with his co-workers S. Funahashi, J. Guo, H. Guo, K. Wang, and A. L. Baker. An initial patent application was submitted in 2015 (US Provisional Patent Application 62/234,389) and several publications appeared between July and August 2016 [63,64,81,135]. The recent published work on CSP has been reviewed by Maria et al. [136], in which they state, 'We define CSP as the process where an inorganic powder is densified in the presence of a transient liquid phase at a phase fraction typically between 1 and 10 vol.-%.' They also stated,

Cold sintering of materials includes using a process of combining at least one inorganic compound, e.g., ceramic, in particle form with a solvent that can partially solubilise the inorganic compound to form a mixture; and applying pressure and a low temperature to the mixture to evaporate the solvent and densify at least one inorganic compound to form sintered materials

and Novel aspects of CSP in comparison to previous works are: (i) the evaporation of the solvent while densifying the material, requiring a processing temperature typically above the boiling point of the solvent and below 300 °C; (ii) the integration with a wide range of thermoplastic polymers; (iii) '1–25 wt-% of liquid for a wide range of solvents, including C1–12 alcohol, ketone, ester, water, or an organic acid or mixtures having a boiling point below 200 °C'.

CSP has been demonstrated to be a powerful tool to engineer microstructures, particularly at the grain boundary level, of hybrid organic–inorganic materials and two-dimensional (2D) materials. CSP allows precise microstructural design of composites, allowing control over their electrical, thermal, and mechanical properties, such as permittivity, electrical breakdown strength, and thermal expansion coefficient [137]. An added benefit of the CSP is in the consolidation of thermodynamically unstable compounds. This has been

well demonstrated by Bang et al. [71] who applied CSP to SnO , a thermodynamically unstable phase undergoing thermal decomposition into SnO_2 and Sn at relatively low temperatures, achieving densification of up to 89% in 100 min under an uniaxial pressure of 350 MPa.

CSP work can be grouped according to the nature of the electrical conductivity of the materials and their applications in different fields, as discussed below.

Dielectric materials (ferroelectrics). Dielectric materials find applications in many electronic components, including filters, couplers, baluns, antennas, and capacitors. Operational devices are composed of multi-layered ceramics, and CSP has opened up the novel possibility of being able to fabricate such devices without the need of a firing step. A demonstrated advantage of CSP applied to dielectrics is the possibility of multi-material integration. Conventional sintering and assembly of a working device requires several steps with repeated heating, including forming (tape casting), multilayer assembly, firing, metallisation of electrodes, integration with a substrate. CSP allows in a single step the integration of organics and inorganics, and it has the potential to surpass conventional processing routes by offering unprecedented 'all in one step' solutions to manufacture devices. It also opens up the possibility of densifying metamaterials with engineered arrangements of dissimilar materials with diverse dielectric properties.

In initial work by Baker et al. [81], they screen printed a paste (milled powder, with poly(propylene carbonate) with Ethylene Glycol Diacetate Butyl Benzyl Phthalate S-16) containing Lithium Molybdenum Oxide powder to produce printed capacitors on nickel and PET foils. The integration of these dissimilar and oxygen sensitive materials (without the need of an inert processing atmosphere) demonstrates a clear advantage of CSP compared to conventional sintering. The ink was deposited and subjected to a uniaxial pressure of 70–100 MPa at room temperature. The materials were dense, and the Li_2MoO_4 capacitors had dielectric properties similar to those of conventionally processed materials.

CSP has also been applied to other ferroelectric materials such as KH_2PO_4 , NaNO_2 , and BaTiO_3 [135]. The properties of KH_2PO_4 and NaNO_2 were found to be comparable to those of conventional sintered materials even when processed at $T < 120^\circ\text{C}$ under 350 MPa without the need of any further treatment. In the case of BaTiO_3 , a further annealing at 900 °C was necessary to complete the consolidation/reaction and achieve properties comparable to conventionally made counterparts (sintered at 1200–1300 °C). The 50 nm starting nanoparticles of BaTiO_3 were consolidated at 180 °C under a pressure of 430 MPa to achieve a relative density of 95%. After annealing at

900 °C in a conventional furnace the relative density remained unchanged, and the dielectric constant reached ~1760 and the loss was 0.03.

$K_{0.5}Na_{0.5}NbO_3$ [138] and $Na_{0.5}Bi_{0.5}TiO_3$ [139] piezoelectric ceramics were prepared using CSP (120 °C, 350 MPa) followed by annealing at 1050–1150 °C. In comparison to $K_{0.5}Na_{0.5}NbO_3$ produced using conventional sintering at 1200 °C, CSP was found to maintain potassium-rich phases in the pressed materials, and enhance green density and sinterability. The reduced sintering temperature of 1145 °C (by ≈ 50 °C) minimised the volatilisation of the alkali metals, contributing to good ferroelectric, piezoelectric, and dielectric properties. Its piezoelectric coefficient, dielectric constant, dielectric loss at 10 kHz, and remnant polarisation and coercive field were 131 pC/N, 10922, 0.0486, 17.3 C cm^{-2} and 8.3 kV cm^{-1} , respectively.

Microwave dielectric ceramics. Microwave dielectric ceramics are employed in modern wireless communication systems as resonators, filters and capacitors [140]. These applications require a permittivity ϵ_r between 15 and 100, a MW quality factor Q_f exceeding 5000, and a near-zero temperature coefficient of resonant frequency. Most of the selected materials (Li_2MoO_4 , $Na_2Mo_2O_7$, $K_2Mo_2O_7$ and NaCl) have good solubility ($> 8 \text{ g L}^{-1}$) in water, resulting in relatively easy full consolidation even at room temperature and a pressure below 200 MPa. These materials are not currently employed as commercial microwave materials. A clear advantage of preparing these materials by CSP was the absence of any undesired inter-diffusion between layers and delamination, which are typical issues during conventional processing.

CSP was used to produce microwave and packaging dielectric substrates in the form of bulk monoliths, multilayers and ceramic–polymer composites [140]. The microwave dielectric properties were comparable with materials prepared using conventional sintering and were selected to demonstrate the feasibility of CSP in microwave and packaging substrate applications [66]. Selected dielectric ceramics could be densified up to 95%. Good microwave dielectric properties (permittivity, 5.6–37.1; Q_f , 1700–30500 GHz) were obtained by CSP processing ($T < 200$ °C, 30–350 MPa) [66].

Bulk $Na_{0.5}Bi_{0.5}MoO_4$ – Li_2MoO_4 [140] microwave ceramic composites were prepared using CSP at 150 °C and 200 MPa for 30 min. A dielectric lens made of functionally graded ceramics was also fabricated. $Na_2Mo_2O_7$ ceramics with polyetherimide (PEI) composites [141] were cold-sintered to realise high performance composites and integrated multilayer circuits. Furthermore, the characteristic dielectric breakdown strength of the ceramic–polymer composite obtained from a

Weibull analysis increased dramatically from 55.1 to 107.5 MV m^{-1} with 10–20 vol.-% PEI additions. In the case of high PEI content, where there was more segregation of the polymer within the ceramic matrix, there was a gradual decrease in the dielectric breakdown strength. A $Na_2Mo_2O_7$ –PEI–Ag bulk ring resonators [141] was obtained by post screen printing. As a prototype of integrated multilayer circuits, $Na_2Mo_2O_7$ –PEI–Ag multilayer ring resonators with good microwave dielectric properties were produced.

Microwave dielectric ceramics have also been prepared using water soluble NaCl samples. The presence of NaCl accelerated the densification of the Al_2SiO_5 –NaCl composite [142]. Comparing dry pressing to CSP, Hong et al. [143,144] found that the presence of water promoted microstructural homogeneity, inducing a much higher Q_f compared to dry conditions. The optimal microwave dielectric properties of $\epsilon_r = 5.55$, $Q_f = 49,600 \text{ GHz}$ and $f = -173 \text{ ppm } ^\circ\text{C}^{-1}$ were obtained for CSPed NaCl ceramic with an applied pressure of 300 MPa at room temperature. Following a similar idea, Induja and Sebastian prepared an Al_2O_3 –NaCl composite [145].

$Li_2Mg_3TiO_6$ [146] ceramics with ultrafine grains were prepared using a CSP followed by post-annealing at 950 °C. Samples CSPed at 180 °C under 300 MPa yielded a high relative density of $\sim 90\%$. Liu et al. correlated Q_f values from 17,790 to 47,960 GHz with different grain sizes of 100–1200 nm.

Semiconductors and proton conductors. Because of its easy processability and wide range of applications, one of the most investigated CSPed materials is ZnO, with 16 papers already published on the material [68,73,147–150]. A new type of ZnO–PTFE (polytetrafluoroethylene) nanocomposite varistor was fabricated by CSP at 285 °C and 300 MPa [148]. The PTFE segregated to the ZnO grain boundaries on a nanometer length scale (1–10 nm) allowing control of the varistor behaviour. Cold sintered ceramic nanocomposites of 2D-MXene and ZnO [73] were fabricated using CSP at 300 °C for 1 h at 250 MPa. The 2D $Ti_3C_2T_x$ MXene was distributed evenly at the grain boundaries, preventing grain coarsening. The addition of up to 5 wt.-% $Ti_3C_2T_x$, contributed to an increase by 1–2 orders of magnitude of the electrical conductivity. Lowum et al. reported the strength of CSPed [151] ZnO using a ball-on-three-balls biaxial bending test method. The samples followed a Weibull distribution with an average strength of 64.4 MPa and a Weibull modulus of 8.

Negative temperature coefficients of electrical resistivity and thermal expansion were reported for cold sintered V_2O_5 ceramics and co-sintered V_2O_5 –PEDOT:PSS composites [152]. Resulting materials had an electrical response comparable to counterparts produced using traditional firing. CSP and co-firing

of multilayer thermoelectric devices was demonstrated by Funahashi et al. [68]; integrated ZnO and $\text{Ca}_3\text{Co}_4\text{O}_9$ (n-type and p-type) multi-layered thermoelectric oxides were fabricated at a sintering temperature below 300 °C, and a PTFE insulator was interposed between the thermoelectric legs.

Nakaya et al. CSPed the proton electrolyte material CsH_2PO_4 [153] at 120 and 200 °C under 300 MPa for 1 h. Significant grain growth occurred during the CSP processing (from 2 to 100 μm), providing an improved ionic conductivity of $2.30 \times 10^{-4} \text{ S cm}^{-1}$ at 200 °C due to the smaller number of grain boundaries and the high crystallinity of the compound.

Battery materials. Recent progress in the development of solid state electrolytes has been reviewed by Liu et al. [154]. CSP clearly has merit in allowing multi-material integration for both liquid and solid electrolyte based batteries, with the possibility to control the intergranular composition being another advantage of CSP. The research on solid electrolytes with high ionic conductivity, good electrochemical stability, and resistance to Li dendrite formation remains an open challenge. A promising approach to overcome this issue is the use of multiple components. Lee et al. [155] prepared ceramic-salt composite electrolytes CSPed at 130 °C under 380 MPa. As a model system, composites of $\text{Li}_{1.5}/\text{Al}_{0.5}\text{-Ge}_{1.5}(\text{PO}_4)_3$ (LAGP) with bis(trifluoromethanesulfonyl)imide (LiTFSI) salts were cold sintered. Ionic conductivities in excess of $10^{-4} \text{ S cm}^{-1}$ at 20 °C were reported [155].

Pereira da Silva et al. compared the ionic conductivity of scandium-substituted NASICON ($\text{Na}_{3.4}\text{Sc}_{0.4}\text{-Zr}_{1.6}\text{Si}_2\text{PO}_{12}$) using Field Assisted Sintering Technology (FAST/SPS) and CSP (250 °C and 300 MPa) [156]. Both techniques allowed the fabrication of electrolytes with electrical resistivity an order of magnitude higher than the ones obtained by conventional sintering because of their small grain size. Leng et al. [157] fabricated a Mg-doped NASICON ($\text{Na}_{3.256}\text{-Mg}_{0.128}\text{Zr}_{1.872}\text{Si}_2\text{PO}_{12}$) solid state electrolyte by CS at 140 °C under 470 MPa to ~83% of its theoretical density. Subsequent low-temperature annealing at 800 °C was found to substantially increase the electrical conductivity to $>0.5 \text{ mS cm}^{-1}$, with a concomitant increase in the grain boundary conductivity. Moreover, annealing at 1100 °C increased the conductivity to $\sim 1.36 \text{ mS cm}^{-1}$ – double that of dry-pressed specimens sintered under the same conditions. The authors noted that processing temperatures below 800 °C opened up new possibilities in the consolidation of ‘thermally-fragile’ ceramic solid electrolytes for both Li^+ and Na^+ . Liu et al. [158] processed using CSP $\text{Li}_{1.3}\text{Al}_{0.3}\text{Ti}_{1.7}(\text{PO}_4)_3$ (LATP) at 120 °C under 420 MPa followed by annealing at 650 °C. They also compared samples prepared using several solvents and reported an increase in

ionic conductivity induced by the nanoprecipitates formed at the grain boundary during CSP.

Berbano et al. fabricated a $\text{Li}_{1.5}\text{Al}_{0.5}\text{Ge}_{1.5}(\text{PO}_4)_3$ solid electrolyte [159] using CSP (20–160 °C 400 MPa). They produced 80% dense electrolytes at 120 °C in 20 min. Post heat treatment at 650 °C resulted in a Li-ion conductivity of $5.4 \times 10^{-5} \text{ S cm}^{-1}$ at 25 °C. Improvement in ionic conductivities up to $1 \times 10^{-4} \text{ S cm}^{-1}$ were achieved using CSP for a LAGP-(PVDF-HFP) composite system sintered at temperatures below 200 °C and soaked in a liquid electrolyte. A clear advantage of CSP is the opportunity to build multilayer battery technology by avoiding thermal degradation and thermal stresses due to the coupling of materials with different CTE (coefficients of thermal expansion).

Seo et al. [160] employed CSP to consolidate LiFePO_4 based cathode composites, achieving dense materials at 240 °C and 600 MPa. The cold-sintered composite cathodes, assembled in a half-cell, exhibited a high volumetric capacity $\sim 340 \text{ mAh cm}^{-3}$ and a gravimetric capacity $\sim 158 \text{ mAh g}^{-1}$. Binderless LiFePO_4 cathodes with high volumetric capacity [161] were also produced.

V_2O_5 and carbon-nanofiber composites were prepared by Heidary et al. [162] at 120 °C (350 MPa, 20 min) for use as cathode materials. They showed that by adjusting the carbon nano fiber loading, the electrical conductivity and volumetric capacity was increased. CS of a covalently bonded (within the S–Mo–S layers) MoS_2 /graphite composite for use as a high capacity Li-Ion electrode was demonstrated, with fabrication of highly dense electrochemically active MoS_2 /graphite composites achieved with a relative density of 88%, using processing conditions of 140 °C, 520 MPa for 60 min [72]. The specific capacity of the composite electrode was $\sim 950 \text{ mAh g}^{-1}$ at 0.1 A g^{-1} . The addition of AHM (Ammonium heptamolybdate) and thiourea allowed consolidation of the MoS_2 phase, which could not be obtained in the presence of water.

3. Materials and general mechanisms of ULES (inter-particle bonding and consolidation)

3.1 Formation of inter-particle primary bond in ULES

In the theory of sintering, consolidation is driven by the pressure gradients between concave and convex surfaces where atomic diffusion is activated. This usually happens at a homologous temperature of $\approx 2/3$ of the melting point (in K), and results in the formation of primary (metallic, ionic, covalent or mixed) bonds between particles. However, the formation of primary bonds (metallic, ionic, covalent or mixed) between sintering particles might even be possible in less demanding conditions of temperature by playing with other

environmental parameters, such as, pressure or the presence of liquid. Also, several types of weak interactions, solid-to-solid and solid-to-liquid [6] exist: Hydrogen, London, Van der Waals bonds, etc. In the 1990s Lee [163–166] explained the mechanism behind solid–solid adhesion as an extension of the more general Hard–Soft Acid–Base (HSAB) Principle. In general, depending on the distance between atoms, it is possible to distinguish between primary and secondary bonds. This section presents an analysis of how primary bonds can form during ULES, and the details are summarised in Table 2.

3.1.1 Formation of primary bonds in dry conditions and consolidation by plastic deformation

In dry (vacuum) conditions, the formation of primary bonds between metal particles is possible in the case of ideally clean metallic surfaces. Cold bonding or cold welding finds technological uses for cold welding of screws, nails and plates (different metals like Ti, Al, etc.) through the removal of the protective oxide at the contacting surfaces. The joining of metals together on the basis of this principle, referred to as ‘cold welding’ [170], is clearly demonstrated in the work of Goldman et al. [15] on Nickel and Nickel-based alloys by applying a pressure of 3 GPa at room temperature. Spontaneous cold welding (pressureless at room temperature) is mostly applicable to noble metals like Au and Ag in the forms of nanowires or nanoparticles [170], but seems to not be applicable to other metals or materials. The formation of primary bonds between particles in dry conditions at room temperature in the case of ionic, covalent or mixed bonded materials is controlled by diffusion, which might be significant even at room temperature for compounds having low melting points. An added complexity in this analysis is the changes in diffusion coefficient with applied

pressure discussed in Ref. [171]. A more exotic way to encourage the formation of bonds near room temperature under dry conditions is through surface activation by ion beam bombardment [172] or cold plasma treatment [173]. The latter is not applicable by definition to the case of ULES.

More work needs to be done to clarify the formation of inter-particle chemical bonds in dry (vacuum) conditions. Only a few works on dry pressing of ionic salts exist, including NaCl and RbI [143]. These compounds possess two independent slip systems active at room temperature, thus enabling dislocation motion, deformation and eventually micro cracking. At least five independent slip systems are required to produce a completely congruent deformation by plastic flow without the formation of voids and cracks. However, these experiments were carried out in air, consequently the powders might have contained a certain amount of residual moisture and so consequently, the results are not conclusive. Further work is needed for a comparative analysis of the effect of dry and liquid conditions on assisted deformation assisted sintering.

CS is mostly applicable to metals or cermets (Figure 7) consolidated at room temperature in dry conditions where plastic deformation is achieved by dislocation motion, and twinning [174]. Densification typically requires very short times, usually < 15 s [175] and it follows the pressure application, where at the beginning of the process the particles rearrange without yielding. With further increasing pressure, localised yielding takes place at the particle-particle contacts, which propagates along the freshly formed grain boundaries as the material plastically deforms, finally resulting in a dense bulk component. Plastic flow requires a minimum volumetric strain energy according to the von Mises criterion. However, some limitations of the model exist as powders are compressible and the yield stress of particulate materials

Table 2. Primary bond characteristics in dry and wet conditions. A similar table, proposed by Alberts et al. in a biology textbook [167], is useful to understand the formation of primary bonds in ULES.

Type of bonds	Metallic	Ionic	Covalent bonding
Bond strength in vacuum/ dry conditions kJ mol ⁻¹	110–350	335–1050	63–1070
Bond strength in water kJ mol ⁻¹	Almost unaffected. Corrosion to be expected	Reduced by more 80 times due to higher permittivity in water ($\epsilon_r = 111$ formamide, $\epsilon_r = 80.1$ water, $\epsilon_r = 1$ air) ^a	Almost unaffected
Solubility in water	Insoluble (corrosion)	Generally soluble, governed by solubility product (K_{ps}) ^b	Insoluble*
Directionality	Non directional, ions surrounded by free electrons	Non directional, complete electron transfer from metal non-metal atoms	Directional, sharing of electrons in the valence shell between non-metals or metalloids
Electronegativity difference	N.A.	>1.7	mixed bonding: 0.5–1.7; pure covalent <0.5

^aCoulomb law (the electrostatic force, F) with permittivity ϵ_r

$$F = \frac{q \cdot q'}{4\pi \cdot \epsilon_0 \cdot \epsilon_r \cdot r^2} \quad (1)$$

^bIonic compounds are in general highly soluble in water or polar solvents. However, some salts are insoluble (concentration < 0.01 M) due to their low solubility product constant (K_{ps}). For example NaCl solubility in water at 50 °C is ~370 g L⁻¹ while AgCl is ~5 mg L⁻¹ [168,169].

strongly deviates from that of the dense material [176–178]. A variety of empirical relationships have been developed to correlate pressure and density [179–182]. Probably, the most accepted equation is the one developed in 1998 by Panelli and Filho:

$$\ln\left(\frac{1}{1-\rho}\right) = A\sqrt{P} + B \quad (2)$$

where P is the applied pressure and A and B are two constants; the former referring to the resistance of the material to plastic flow, with the latter depending on the tap density. An application of Equation (2) is reported below in Figure 8. A more empirical relationship [12] suggests that the maximum achievable density ρ_{lim} of a material follows the relationship

$$\rho_{lim} = 1 - e^{\frac{-3P}{2\sigma_y}} \quad (3)$$

where σ_y is the yield stress. According to this relation, a relative density of 98.9% is achieved when $P = 3\sigma_y$ and a density of 99.75% when $P = 4\sigma_y$.

3.1.2 Inter-particle primary bond formation in the presence of a liquid: ionic and covalent bonded materials

Referring to Table 2, under dry conditions, excluding thermally activated diffusion (applicable to materials with melting points of < 900 K) [12], it is difficult to achieve the formation of primary bonds between particles in ionically or covalently bonded materials. Raymond Franssen [183] (1993) reported that dry sodium chloride grain boundaries are essentially immobile – suggesting very limited diffusion – at temperatures below 400°C . This is in contrast to the accelerated grain boundary migration in the presence of water even at room temperature [184]. It is well established that the presence of a liquid promotes the formation of inter-particles bonds with a strength well exceeding those of Van Der Waals bonds as discussed in Ref. [10] (see Section 1.2).

A parameter of primary importance in wet ULES is the solubility of the powder in water/liquid. Solubility constants describing the combination of common cations and anions are available in solubility tables and dedicated handbooks [168,185]. Because the amount of water is below 10 vol.-%, consolidation in wet ULES is typically achieved by partial solubilisation rather than complete solution precipitation as in the case of evaporites [186].

When a solid substance is in contact with a liquid, four different phenomena can be observed: (1) dissolution; (2) chemical reactions; (3) absorption limited to the surface; (4) electrostatic/steric repulsion/wetting. The first two are favourable in promoting consolidation in ULES. Solvates formed from the interaction between solvent and solute might have profoundly different physical and chemical properties from those

of the starting parent materials. Such differences might explain why, in some instances, sinterability only occurs in the presence of a liquid rather than in dry conditions. In ULES any liquid could be employed, the liquid should be selected accounting for processability (solubility, evaporation temperature) and targeted chemical reactions.

Another way to describe solvation and hydration is through the free energy change of both solute and solvent. The process is parameterised through the standard molar Gibbs free energy of new compound formation (ΔG_f°), which expresses the change in the Gibbs free energy [187–189]. The ΔG_f° of hydration is known for several materials [187] at 1 atm and 298.15 K. External pressure in CSP and HHP processes might affect these values as theorised in Ref [190]. Hygroscopic compounds tend to chemically absorb water on the surface of their particles, suggesting the possible formation of secondary phases that could play a significant role in accelerating consolidation.

The solubility limit plays an important role in CS. Once this equilibrium limit is achieved, the solvent is unable to dissolve any more species from the suspended particles. The solubility of some of the most important materials processed by wet ULES are presented in Table 3.

The solubility limit can also be affected by external physical conditions, such as temperature and pressure [212,221,228], and internal chemical parameters (pH and the nature of the solvent). The higher the solubility limit the higher the quantity of dissolved species taking part in the sintering. The interphase formed between the sintering particles can be either amorphous or crystalline, and detailed analysis of the formed interphase is scarce in the literature. Schenk and Urai [184] studied the interphase that formed in NaCl using cryo-SEM, allowing a complete identification of water-rich boundaries that would not be possible using conventional SEM. Such inter-particle boundaries are highly mobile in the presence of a water-rich phase (brine or film). In wet ULES the use of additional heating might contribute to the drying of these grain boundaries. Further work should be dedicated to understanding the relationship between the nature of grain boundaries (i.e. crystalline or amorphous), their thickness and processing parameters (pressure application, temperature, heating and cooling rates) on the grain boundary characteristics. The nature of grain boundaries in samples made by wet ULES can be distinctly different to those processed by conventional means.

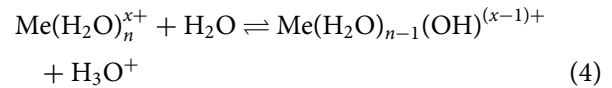
The thermodynamic stability of cation–ligand complexes is governed by the properties of the ligands, ions and the type of bonding. The cation–ligand interaction is an example of the Lewis acid–base interaction. [163] Lewis bases (ligands) can be divided into two main categories:

Table 3. Processing route, solubility, ionic species.

Material	Process	Solubility in water at 25 °C (g L ⁻¹)	Ionic species	Comments/feature	Ref.
CaCO ₃ Nano-CaCO ₃	HHP	1.3 × 10 ⁻²	Ca ²⁺ , CO ₃ ²⁻ , HCO ₃ ⁻	Salt compound – strong base/weak acid	[191,192]
SiO ₂ – Amorphous	CSP – HHP	3.9 × 10 ⁻²	SiO(OH) ₃ ⁻ , SiO(OH) ₂ ⁻	Extensively used in other low temperature processes of densification	[193–196]
SiO ₂ – Quartz	CSP – HHP	2.9 × 10 ⁻³	SiO(OH) ₃ ⁻ , SiO(OH) ₂ ⁻	Processed mostly in alkaline environment	[196–198]
NaCl	CSP	357	Na(H ₂ O) ₄ ⁺ , Cl ⁻	Salt compound – strong base/strong acid	[199,200]
NaNO ₂	CSP	820	Na(H ₂ O) ₄ ⁺ , NO ₂ ⁻	Salt compound – strong base/weak acid	[201]
WO ₃	CSP	insoluble	WO ₄ ²⁻	Almost totally stable in water – it could only be superficially hydrated	[202,203]
ZnO	CSP	6 × 10 ⁻⁶	Zn(H ₂ O) ₆ ²⁺	Highly dissolvable in acetic acid solution or biological buffers	[204–206]
V ₂ O ₃	CSP	0.1	[VO ₂ (H ₂ O) ₄] ¹⁺	Less stable metal oxide due to the r/s – 8	[207–209]
V ₂ O ₅	CSP	8	[VO(H ₂ O) ₅] ²⁺	Solubility enhances as the valence increases (r/s > 8)	[207–211]
MgO	CSP	6.2 × 10 ⁻⁵	Mg(H ₂ O) ₆ ²⁺	Quite stable in water – r/s ~ 3	[212–214]
ZrO ₂	CSP	Negligible	[Zr(OH) ₂ ·4H ₂ O] ₄ ⁸⁺ , [HZrF ₆] ⁻	Highly stable metal oxide - dissolvable in HF	[215–216]
TiO ₂	HHP	Insoluble	As for Zr plus Ti(OH) ₅ ²⁻ , Ti(OH) ₆ ⁻	The hydrophobicity renders this material insoluble in water – when hydrophilic it is the most stable metal oxide	[217–219]
BaTiO ₃	CSP – HHP	Insoluble	Ba ²⁺ , Ti(OH) ₅ ²⁻ , Ti(OH) ₆ ⁻	Titanium hydrates at high temperatures tend to form TiO ₂ prior reaction with Ba ²⁺	[83,220]
MoO ₃	CSP	4.9(28 °C)	MoO ₄ ²⁻ , Mo ₂ O ₇ ²⁻ , Mo ₂ O ₃ ⁺ , MoO ₃ ⁺ , MoO ₂ ²⁺	Protonisation produces several cations	[221–225]
Li ₂ MoO ₄	CSP	82.6	Li ⁺ , MoO ₄ ²⁻	Reduction (in acid media) produces many molybdate salts	[224,226,227]
Na ₂ Mo ₂ O ₇	CSP	8.4	Na ⁺ , Mo ₂ O ₇ ²⁻		[224]
K ₂ Mo ₂ O ₇	CSP	15.3	K ⁺ , Mo ₂ O ₇ ²⁻		[224]

1. Hard bases, including small, relatively non-polarisable donor atoms (e.g. C, N, O, and F);
2. Soft bases, containing larger, relatively polarisable donor atoms (e.g. P, S, Cl, Br, I).

Based on the soft–hard definition [163], we can explain why in nature most first-row transition metals are isolated as oxide ores (hard nature), while copper, zinc and most of the second- and third-row transition metals occur in nature as sulfides (soft nature). Atoms in the periodic table [229] can be grouped as hard cations (all electrons removed from the outer shell), like Na⁺, K⁺, Mg²⁺ shown in Figure 6 (a), intermediate cations (some electrons remain in the outer shell), early transition metals cations and hard–soft anions. Dissolved metal ions form metal aquo complexes with the general formula Me(H₂O)_n^{x+}, in which oxygen atoms of the water molecules form covalent bonds with the metal ion. Unavoidably aquo complexes tend to hydrolyse by the following acid–base reaction as described by Richens [230].



As a matter of fact, very weak acids, such as Na⁺ and K⁺ ($z/r \sim 1$) show an almost imperceptible hydrolysis. Divalent ions with a large radius, such as Ca²⁺, Zn²⁺, and Pb²⁺ non metal ions with five of higher oxidation states forms oxo-ion. For example vanadium (V) ion V⁵⁺ ($z/r \sim 8$) forms VO²⁺ cation and the resulting aquo oxo-ion complex has the following structure [VO(H₂O)₅]²⁺.

Hydrolysis is directly correlated to the ionic potential of metal ions, however, it can be suppressed by acidification of water if necessary to avoid species precipitation during CSP. For example, the CSP of ZnO occurs in acid solution because it limits hydrolysis, see Equation (4). The mechanism of dissolution precipitation preferentially involves the aqua complex Zn(H₂O)₆²⁺ instead of hydroxides. Aqua complexes and metal hydroxides can be dehydrated by thermal treatment at a range of temperatures from 50 °C to 600 °C. Low hydrolysable CuBr₂·4H₂O becomes anhydrous below 100 °C while NaOH is converted to Na₂O above 500 °C. The presence of water can be expected in wet ULES materials if the dehydration temperature exceeds the sintering temperature. In such cases, further heat treatment might be necessary to completely remove water. Conversely, CSP is rarely reported for species that undergo extensive hydrolysis, e.g. Be²⁺ ($z/r \sim 8$), Fe³⁺ ($z/r \sim 6$) or Al³⁺ ($z/r \sim 8$).

As presented in Figure 6, the solubility of hard cations is linked to the ratio of ionic charge to ionic radius (z/r), known as the ionic potential. As shown in Figure 6 (a), hard cations with an ionic potential of 1⁺ in water like Li⁺, Na⁺, K⁺, tend to form hydrated

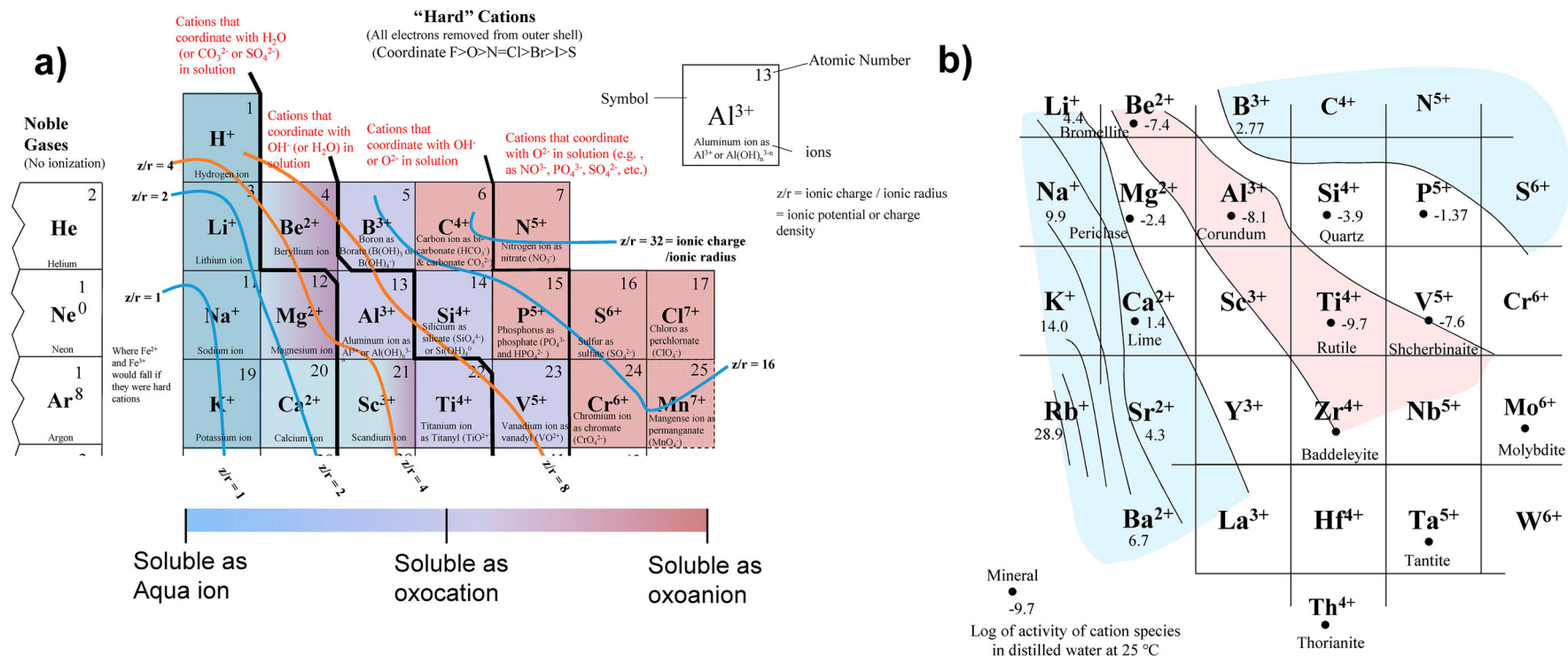


Figure 6. (a) Aqueous geochemistry and speciation of ‘Hard’ (also referred to as ‘Type A’) Cations (All electrons removed from outer shell). Extract of periodic table from an Earth Scientist’s Periodic Table [229]. Ionic potentials follow the order F > O>N>Cl>Br>I>S (isolines). (b) Logarithm of the solubility of their oxide in water at 25 °C [229].

cations (aquo-ions), whereas hard cations of ionic potential of 2 and 3 like Mg^{2+} , Ca^{2+} , Be^{2+} , Al^{3+} , Si^{4+} form hydro complexes like BeOH^+ , $\text{Al}(\text{OH})_4^{3-n}$, SiO_4^{4-} , $\text{Si}(\text{OH})_4^0$. The coordination number, n , of a substance with water ($n\text{H}_2\text{O}$) depends strongly on thermodynamic properties such as the ionicity of the bond, the cation's electronegativity, the ionic radius, and the volumetric water capacity [231]. The polynuclear hydrolysis products are unstable ions (i.e. $\text{Zr}_4(\text{OH})_8^{8+}$) which have a tendency to precipitate and hinder sintering (not promoting mass transport).

For oxides and fluorides, higher solubility occurs for weak cation to anion attraction (low ionic potential of the cation or large ionic radius). For nitrates and sulfates high solubility corresponds to high ionic potential. This behaviour is for complexes of halides of silver, mercury (soft cations), sodium and magnesium (hard cations) (see inset 8 in Ref [229]). In Figure 6 (a) hard cations are grouped with respect to their coordination (see red text), suggesting a relationship with the preferred anions (OH^- , NO_3^- , PO_4^{3-} , SO_4^{2-}) for promoting dissolution in wet ULES. This, for example, is consistent with the enhanced solubility of SiO_2 in a basic environment.

The ionic potential expresses the density of charge of each ion and it is considered to be a useful parameter to normalise its 'ionic strength', i.e. how strongly it attracts oppositely charged ions, repels like-charged ions, and how easily the ion can interact with O^{2-} (or other anions) to form stable bonds [229]. A relationship between ionic potential and solubility of the oxides was presented by Railsback in 2003 [229]. Figure 6(b) reveals that the highest stability and reduced solubility is displayed for oxides with metal ions having an ionic potential falling in the range 4 to 8. Group IV metal oxides indeed, are among the least soluble metal oxides, showing the lowest amount of dissolved ionic species, see Figure 6(b). Outside this range, the solubility limit and kinetics of materials increases (see V_2O_5 and silica based compounds in Table 3).

For ionic substances, the higher the permittivity of the solvent (ϵ), the greater the ability of the solvent to dissolve an ionic lattice by decreasing the intermolecular energy of ions and polar substances. Since the strength of an ionic bond follows Coulomb's Law, it is directly proportional to the product of the charges on the ions, inversely proportional to the square of their distance, and inversely proportional to the dielectric constant of the solvent [232,233].

The ability to 'dissolve' a solid should not be confused with solubility. Dissolution of a covalent network solid implies the breaking of covalent bonding or chemical reactions between solute and solvent, e.g solvolysis (hydrolysis for water). The dissolution of a pure covalent network is an irreversible process, and only few examples in the literature are reported for wet

ULES of covalent materials. For some materials insoluble even in strong acid or alkaline conditions, CSP is still applicable but the formation of the supersaturated liquid, needed to trigger the densification, is reached by tailored chemical reactions paths. It is possible to play with the chemistry of the solvent, which determines the solubility, the rate of dissolution and the nature of the dissolved species. For example, ZrO_2 has different dissolution dynamics if suspended in HF, HNO_3 or H_2SO_4 [215,234,235]. Or it is possible to pre-load the ionic species in the solvent. For example, $\text{Y}_{(\text{aq})}^{3+}$ ions have been obtained by dissolution of $\text{Y}(\text{NO}_3)_3$ in water [136,236]. Another example of pre-loading was used for covalent bonds, such as MoS_2 /graphite composites which were cold pressed at 520 MPa for 1 h and reached a density of 90%. In this case, the dissolution of Mo and S inorganic/organic precursors in water contributed to the formation of covalent bonds [72]. Using a similar approach, diamond film was formed starting from 1,1,1-trichloroethane under alkaline HHP conditions (≈ 1 GPa, 10 M NaOH, 300 °C, in the presence of a catalyst) compacted using diamond-substrates.

The use of a water based solvent might result in the formation of hydroxides during wet ULES, which would require temperatures well above 300 °C to convert the desired oxide phase, as in the case of ZnO [147]. To avoid the formation of undesirable hydroxides (due to hydrolysis) the use of non-aqueous liquids in CSP is desirable but is limited to a few stable molecules. Dimethyl sulfoxide (DMSO), ketones and dimethyl formamide (DMF) are some examples of polar aprotic solvents able to dissolve cations avoiding hydrolysis. C1-12 alcohols, carboxylic acids and nitro compounds belong to the class of protic solvents. Hong et al. [237] have shown the CSP of low permittivity metaboric acid using ethanol as protic non aqueous solvent obtaining better results than by dry CSP. DMSO has been attempted with good results in the CSP of ZnO and MnO by Kang et al. [147].

Table 3 reports the solubility at 25 °C and the resulting ionic species for several ceramics which are typically processed using ULES in presence of an aqueous solution. The efficiency of the HHP and CSP reactions is related to both the solubility limit and the kinetics of dissolution. Different allotropic forms could have different solubility limits, such as for amorphous silica and quartz [193,197] (see Table 1). The pH of the solvent also strongly affects the dissolution kinetics – for instance, lower values of pH increase the kinetics of dissolution of ZnO in aqueous solution [204,238,239]. Similarly, the size of the particle increases the velocity of the reaction, as the k coefficient is directly proportional to the surface area of solid particles [240–242]. The data reported in the

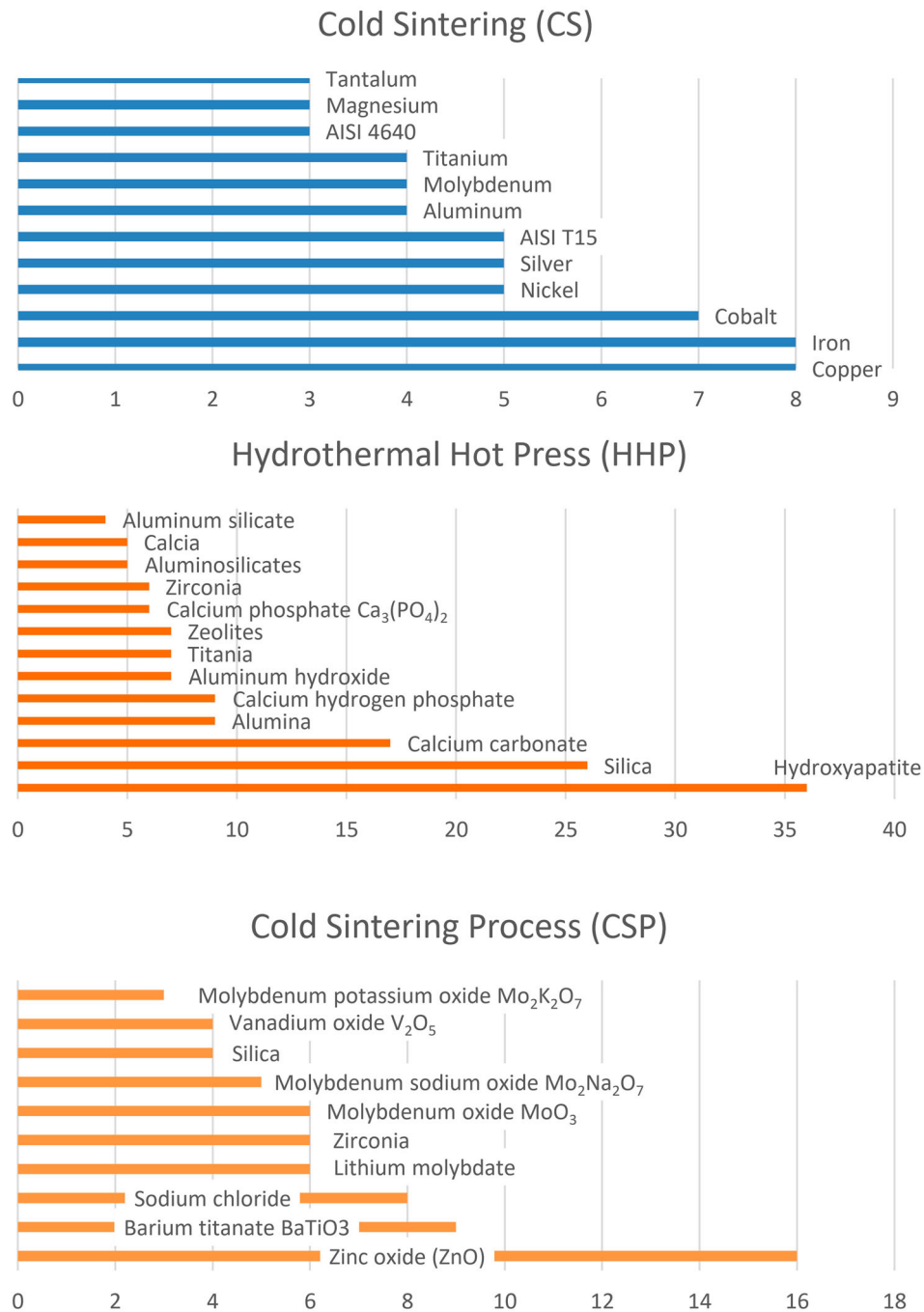


Figure 7. Cumulative number of papers of typical materials processed using CS, HHP and CSP. According to Marie et al. [136], more than 50 materials have been processed using CSP. Considering the chemical composition presented in Table 1 and their combinations (metals/ceramics and organics/ceramics) the list of materials processable by ULES could become endless.

table matches well with the distribution of papers shown in Figure 7.

3.2 Theory of sintering applied to ULES

It is worth recalling that sintering is controlled by a thermodynamic factor (driving force) and by a kinetic factor (atomic mobility). The driving force is a gradient in the chemical potential of atoms induced by pressure differences at the microstructural level, driving material to the neck surface. In conventional sintering these pressure gradients are caused by surface tensions and

curvature. In ULES, in particular HHP and CSP, the application of an external pressure during room temperature consolidation therefore has the effect of increasing this driving force.

The external pressure is also expected to modify the solubility of the ceramic system [243] according to:

$$S_p = S_0 \exp\left(P_{ext} \frac{(\Omega_s - \Omega_l)}{RT}\right) \quad (5)$$

Where S_0 and S_p are the solubility in the absence and presence of an external pressure (P_{ext}), respectively; Ω_s and Ω_l are the molar volume of the solid and the

apparent molar volume of the solid dissolved in the liquid, respectively; T is the absolute temperature and R is the perfect gas constant.

The application of an external pressure (P_e), is expected to clearly increase the solubility at the inter-particle contact point as depicted in Figure 8 (a) because of constriction effects. This aspect is discussed in more details in Ref. [246]. However, exceptions exist where the solubility decreases as pressure increases. The most important factors affecting $\Omega_s - \Omega_l$ are the differences between the compressibility of the solvent and the solute and the polarity of the system, substances dissolved as ions in polar liquids usually exhibiting $\Omega_s - \Omega_l > 0$ (and thus pressure-enhanced solubility) [247]. Since CSP and HHP are in general carried out using water as a solvent, this results in a solubility increase with the pressure. Exceptions are for instance represented by systems containing molten silicates and solid silicate minerals, where the solubility decreases with the pressure [247]. Similarly, the solubility can be enhanced by increasing the temperature of the system. However, opposite trends are seen for a number of compounds like calcium chromate, calcium carbonate, calcium hydroxide, calcium sulfate and cerous sulfate [248].

Nano sized particles are subjected to strong internal stresses ($\sigma = 2\gamma/r$, where r is the particle size and γ the surface tension) due to the surface tension. The solubility of the particulate, by reducing the radius, is therefore enhanced by a factor $\exp(2\gamma\Omega_s/rRT)$ given by the Ostwald-Freundlich equation. This effect is significant for very small particles, and for 15 nm particles the solubility is increased by several folds (even up to 10 times), and the resulting solution is unstable and Ostwald ripening will occur. These sizes, even if they are significantly smaller than the typical particle size in ULES, might still play a significant role in mass transport during sintering [249]. Future work should be dedicated to these unknown aspects.

The sintering mechanisms active during ULES, both on the atomistic and particle size scale, are the subject of continuing debate. Whereas the mechanisms leading to metal powder compaction during dry cold pressing in CS are quite well established (see Figure 8(b)), open questions remain concerning the role of water in HPP and CSP. Using atomistic simulations Sengul et al. [249] suggested hydroxylation during CSP in the presence of acetic acid solution, which generates surface complexes, accelerating the surface diffusion by an order of magnitude.

An overview of the possible sintering mechanisms active during near room temperature consolidation is

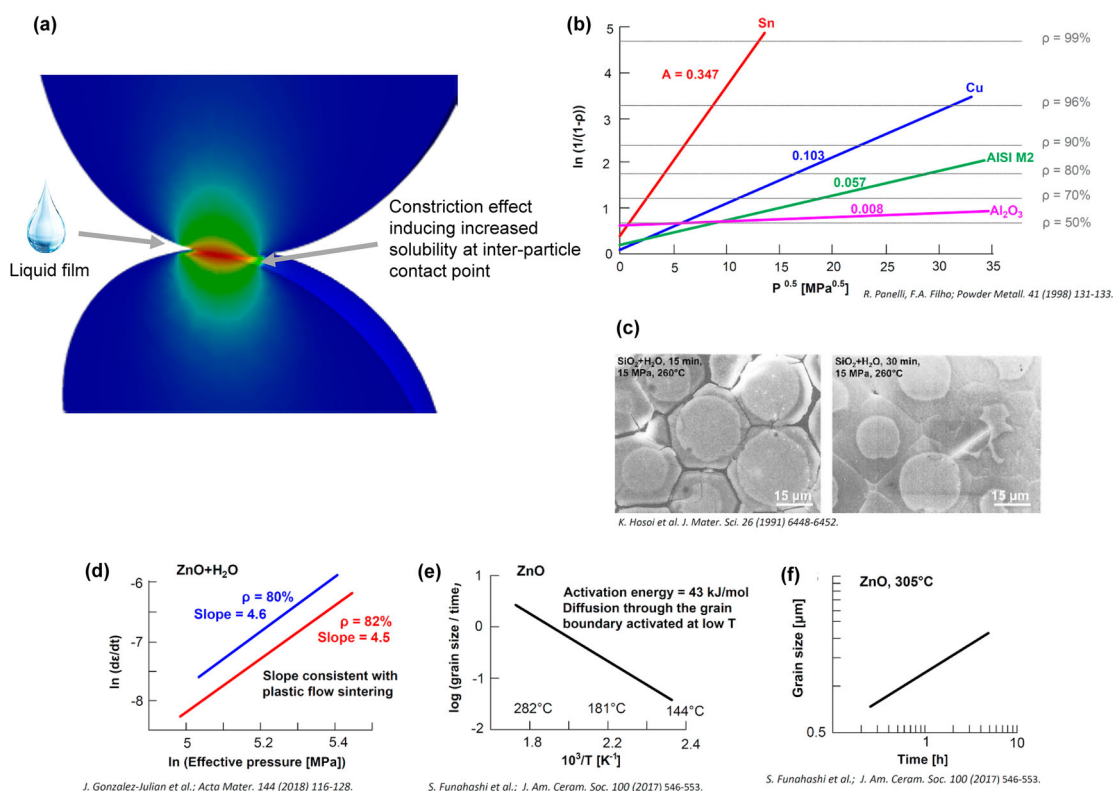


Figure 8. An overview of the room temperature consolidation mechanisms in metals and ceramics: (a) Hertzian contact between two sintering particles showing an increased stress at the contact point which might contribute to increased solubility at the neck during ULES; (b) Application of the Pannelli and Filho equation applied to several dry pressed materials (adapted from [179]); (c) formation of a hydrated layer during HHP of silica (taken from [244] and re-printed with the permission of the editor); (d) sintering kinetics during CSP of ZnO showing plastic flow sintering (adapted from [245]); (e) and (f) grain growth kinetics in ZnO during CSP, indicating that grain boundary diffusion is activated even at low temperature (adapted from [204]).

presented in Figure 8. Densification requires atomic flow from the neck centre to its surface; thus, it requires mass transport phenomena to be activated. Mass transport can take place through plastic flow (i.e. dislocation motion and twinning in CS), viscous flow or atomic diffusion. Indeed, solid state atomic diffusion in metals and ceramics at room temperature is unlikely in most cases because of the relatively large energy barrier for diffusion (usually of the order of a few hundreds of kJ mol^{-1}). Diffusion can, however, be activated in the liquid phase or in highly defective interfaces resulting from the reaction between the liquid and the solid. From this point of view, the addition of a liquid phase is expected to change the kinetics of sintering rather than its thermodynamics.

Theoretical mechanisms of consolidation have been discussed in a separate paper in the case of wet conditions (CSP/HHP) [246]. The work suggests that consolidation does not follow conventional liquid phase sintering (LPS) based on pressure-assisted dissolution in liquid water (in the neck centre) and precipitation (in the neck external surface). The limited knowledge in material science on mechanisms of consolidation in wet ULES could clearly benefit from the deeper understanding in geology, which uses NaCl as a model system. Fluid assisted grain boundary migration has been demonstrated by Schenk and Urai [184] to be effective in reducing dislocation density in NaCl. Dislocations can be annealed out even at room temperature because their stored elastic energy is sufficient to drive the process. Dislocation creep process takes place within the crystal lattice of the halite grains, and this mechanism becomes even more effective when water generates interactions within the bulk of a grain. Solution precipitation creep, or 'pressure solution', is a process, which occurs at the grain boundaries, and therefore relevant to sintering. Schutjens and Spiers [250], using contact dissolution analysis, reported that in the presence of a small amount of grain boundary brine (saturated NaCl solution), atoms dissolve at highly stressed boundaries, and diffuse through the fluid towards less stressed areas where they crystallise. This process results in intergranular sliding and rotation (grain rearrangement), and it has been demonstrated to be responsible for the compaction of salt particles [184,251].

In synthesis the mechanisms operating during CSP/HHP, they are not limited to dissolution/re-precipitation processes through a liquid phase. They are expected to be various and dependent on the interactions between the solvent and the material to be sintered. These mechanisms could involve:

- (i) *Liquid-assisted lubrication.* The presence of water facilitates the sliding, rotation and rearrangement of grains. This is expected to occur in the initial part of sintering and represents a key feature of

any LPS process [243,252]. However, this mechanism only has the effect of increasing the initial density of the compact and does not produce real sintering with neck formation.

- (ii) *Formation of a thick second phase on the powder surface.* The formation of a hydrated (or any reaction with other liquids) second phase on the particle surface causes plastic flow sintering under the effect of the external pressure. Hydrated compounds usually have a relatively low plastic flow stress. However, to attain high densification levels the hydrated layer should be thick enough to accommodate the sintering deformations. This is the case for silicate glass spheres processed under hydrothermal conditions, where a hydrated layer of several micrometres forms in a few minutes at 260°C by a reaction with water [244] (Figure 8 (c)). These effects are accelerated in a caustic environment [253]. Here a key role involves the free energy of hydration of the oxide [190], which governs the formation of the corresponding hydroxide. Other factors that are expected to influence the hydroxide formation are its morphology, its solubility and permeability by water.

- (iii) *Formation of lattice disorder by water-material reaction.* Lattice defects can be formed by the interaction between water and the material on the particle surface. As sintering proceeds, and surfaces are converted to grain boundaries, defects are expected to concentrate in these regions. Defects might influence the local grain boundary diffusivities and plastic flow stresses. Liquid penetration from the surface of the particle toward its core might be accelerated by micro cracking [254] under the applied pressures.

Gonzalez-Julian et al. [245] pointed out that the formation of protonated disorder at the grain boundaries of ZnO during CSP ($2\text{H}_2\text{O} + \text{O}_\text{O}^\times + \text{V}_\text{O}^\bullet \rightarrow 2\text{OH}_\text{O}$) facilitates densification by grain boundary sliding or plastic deformation [245] (Figure 8(c)). The pivotal role of such densification mechanisms was also confirmed by the measurement of a non-linear densification rate vs. pressure relation, which cannot be accounted for by LPS, but is instead consistent with plastic deformation [245]. The presence of 'special' grain boundaries in CSPed ZnO is also supported by Funahashi et al. [204], who observed unexpected grain growth kinetics at only 305°C (Figure 8 (e,f)). Grain coarsening was strongly accelerated in CSP and governed by a very low activation energy: 43 kJ mol^{-1} , instead of $\sim 200 \text{ kJ mol}^{-1}$ for conventional sintering. In other words, ZnO produced by CSP has an activation energy for diffusion through the grain boundary of about 20% of the theoretical value. While this is a very rough approximation (not

accounting for the diffusion pre-exponential constant), it does suggest that diffusion through grain boundaries may well be activated during CSP. If one also assumes a similar decrease in the activation energy for diffusion parallel to the grain boundary, then, it is even more probable that grain boundary diffusion-based sintering is activated during CSP of ZnO.

- (iv) *Liquid-assisted dislocation motion and recrystallisation.* Plastic deformation by dislocation motion appears to have a dominant effect in some alkali halides in the presence of water as also confirmed by Kingery et al. [255]. Here the authors concluded that although LPS cannot be completely ruled out, a pivotal role during densification is played by plastic flow, which is strongly accelerated by the presence of water. The origin of this enhancement is not completely clear, but might be linked to some geological studies on rock salt creep by Urai et al. [251]. They found that even a few ppm (> 10 ppm) of adsorbed water brine at the grain boundary of natural rocks favours dynamic recrystallisation processes, which reduce the dislocation density and the plastic flow stress (reduction of the order 25–50% [251]).
- (v) *Liquid phase-assisted pore shape modification.* Water is expected to accumulate in porosity. There it accelerates mass transport from convex to concave pore surfaces (thus promoting neck growth). However, this kind of mass transport (analogous to surface diffusion-controlled sintering) does not produce densification, as the total pore volume does not change. It only produces a modification of the pore shape. This phenomenon appears quite similar to crystal caking, where hygroscopic salts tend to agglomerate forming solid lumps [256].

Other phenomena take place beyond sintering in CSP and HHP, especially if the water load is high enough to produce a ceramic suspension in the early stages of the process; these are associated with Ostwald ripening and re-crystallisation. The ULES temperatures and pressures are expected to increase the solubility of ceramics, thus accelerating mass transport phenomena as in hydrothermal crystal growth. This results in accelerated coarsening mechanisms (Ostwald ripening). On the other hand, the possibility of dissolution and re-precipitation might allow the formation of new phases, as in the case of the natural formation of quartz crystals due to the dissolution and re-precipitation of volcanic silicate rocks [257].

Conclusions and future trends

A key aspect of Ultra-low energy sintering (ULES) is the reduced (even exceeding 90%) external energy requirement (and associated CO₂ footprint) compared

to conventional sintering processes, and consequently its potentials as a sustainable manufacturing process for advanced materials. ULES could replicate biomineralisation and lithification processes, which are the greenest way of producing ceramics and their composites. The versatility of ULES opens up the possibility of 'all-in-one-step' consolidation of inorganics and hybrid organics/inorganics to produce advanced functional devices (sensors, batteries, 5G antennas, meta-materials, multi-layer capacitors and bio-composites). The low processing temperature brings other advantages, such as suppression of volatilisation of hazardous elements seen in conventional processing, elimination of heat distortion, avoidance of thermal decomposition/degradation, thus paving the way for unexplored inter-particle grain boundary design.

While the process is defined by four main parameters – liquid, powder, heat and pressure – it involves complex and partially unknown phenomena. It is proposed that a synergistic knowledge-base, ranging from material science and engineering to palaeontology, from physics to chemistry could aid our understanding of these techniques to advance their technological/scientific impact. Unlike conventional firing techniques, ULES offers the unprecedented opportunity to integrate sintering with biology, chemistry, geology and engineering. A multidisciplinary scientific approach in understanding ULES could provide a paradigm shift in materials processing leading to a significant impact on the energy, health and environmental sectors.

A survey of different techniques related to ULES suggests different effects in dry, wet and hydrothermal conditions. The comparative analysis allows us to build a general understanding and promote the development of hybrid techniques, where the amount of liquid related effects can be modulated during each stage of sintering.

Several fundamental questions related to ULES still remain open. The particle surface modification induced by a pressurised liquid, which is clearly a distinctive feature of ULES, remains rather unexplored. We have limited understanding about the inter-particle grain boundary formation during sintering, which is essential in order to control the chemistry, stoichiometry, microstructure and atomic ordering of the final body. Considering the different ULES techniques, we are still unable to rationalise the processing parameters (pressure, temperature, time and amount of liquid) during different stages of sintering. Apart from plastic deformation induced effects, without any doubt, the presence of liquid is a key parameter to accelerate densification in ULES. However, liquid drying rate, which is currently poorly controlled during sintering, is expected to push the development of experimental setups with improved control and reproducibility. Taking inspiration from nature (bio-

mineralisation, lithification, evaporites), future work should clearly suggest alternative approaches to enhance ULES densification by replacing the use of brutal forces (≈ 0.5 GPa), which are only applicable to small samples (≈ 10 mm diameter), with a more gentle approach possibly based on prolonged pressing times (from minutes to tens of hours) and more optimised chemical reactions during sintering. Future work should use model systems to build sintering models able to capture the dynamic evolution of liquid-assisted ULES. A deep understanding of past work allows us to define working principles and the potential of the technique. The lack of understanding of the sintering mechanisms from the material science perspective can be addressed through established knowledge in the field of geology where plasticity, grain boundary mobility and recrystallisation have been investigated for many years.

In the future, mass production of ceramics using ULES is expected to provide a significant breakthrough in establishing a greener manufacturing route, while opening the door to new materials and applications. The exponential growth of research into ULES is expected to support the development of a wide range of functional materials; this can only be achieved by understanding the triangle of processing-microstructures-properties. Materials properties can be tailored at the grain boundary level by identifying a suitable liquid ('a sauce') able to engineer chemical composition, grain boundary mobility and degree of crystallisation.

Disclosure statement

No potential conflict of interest was reported by the authors.

Funding

This work is supported by the Thousand Talents Program of China and Sichuan Province. A.I.D. acknowledges support from the STFC Hartree Centre's Innovation: Return on Research programme, funded by the UK Department for Business, Energy & Industrial Strategy. MJR would like to acknowledge the EPSRC Programme Grant XMAT (EP/K008749/2).

ORCID

Mattia Biesuz  <http://orcid.org/0000-0002-4338-4177>

References

- [1] Ashby M, Johnson K. Materials: The stuff that surrounds us. *Mater design*; 2014. p. 62–98.
- [2] Nath AJ, Lal R, Das AK. Fired bricks: CO₂ emission and food insecurity. *Glob Challenges*. 2018;2:1700115.
- [3] Sohrabi Baba Heidary D, Lanagan M, Randall CA. Contrasting energy efficiency in various ceramic sintering processes. *J Eur Ceram Soc*. 2018;38:1018–1029.
- [4] Faouri SS, Mostaed A, Dean JS, et al. High quality factor cold sintered Li₂MoO₄BaFe₁₂O₁₉ composites for microwave applications; 166; 2019.
- [5] Saitta ET, Kaye TG, Vinther J. Sediment-encased maturation: a novel method for simulating diagenesis in organic fossil preservation. *Palaeontology*. 2019;62:135–150.
- [6] Kendall K. Theoretical aspects of solid-solid adhesion. *Sci Prog*. 1988;72:155–171.
- [7] Kendall K, Kendall M, Rehfeldt F, et al. Phenomenology of adhesion: from macro- to nano-systems. In: *Adhesion of cells, viruses and nanoparticles*. Dordrecht: Springer Netherlands; 2010. p. 21–43.
- [8] Brill R, Melczynski I. Hydrothermal sintering. *Angew Chemie Int Ed English*. 1964;3:133–133.
- [9] Turba E, Rumpf H. Zugfestigkeit von Preßlingen mit vorwiegender Bindung durch van der Waals-Kräfte und ihre Beeinflussung durch Adsorptionsschichten. *Chemie Ing Tech*. 1964;36:230–240.
- [10] Turba E, Rumpf H. Tensile strength of pressed compacts chiefly bonded by van der Waals forces and influence exerted by adhesion layers. *Silic Ind*. 1965;30:409–422.
- [11] Hirano S-I, Somiya S. Hydrothermal reaction sintering of pure Cr₂O₃. *J Am Ceram Soc*. 1976;59:534–534.
- [12] Gutmanas EY, Rabinkin A, Roitberg M. Cold sintering under high pressure. *Scr Metall*. 1979;13:11–15.
- [13] Gutmanas EY, Rabinkin A, Roitberg M. On cold sintering of metal-bonded diamond composites. *Mater Sci Eng*. 1980;45:269–275.
- [14] Gutmanas EY, Premkumar M, Lawley A. Microstructure and mechanical properties of cold sintered P/M aluminum alloys. *Prog Powder Metall*. 1984;39:669–682.
- [15] Goldman DB, Gutmanas EY, Zak D. Reduction of oxides and cold sintering of water-atomized powders of nickel, Ni-20Cr and Nimonic 80A. *J Mater Sci Lett*. 1985;4:1208–1212.
- [16] Gotman I, Gutmanas EY. Joining of P/M high speed tool steel with cobalt and ferrous alloys by high pressure consolidation. In: *Proc Horiz Powder Metall Proc Int Powder Metall Conf Exhib; Schmid*. 1986;2:703–706.
- [17] Gutmanas EY, Goldman DB, Clark JB, et al. Cold sintered stainless steel–chromium oxide composites. *Prog Powder Metall*. 1986;41:631–640.
- [18] Gutmanas EY, Goldman DB, Hart S, et al. Cold sintered 4640 steel–vanadium carbide composites. In: *Proc Horiz Powder Metall Proc Int Powder Metall Conf Exhib; Schmid*. 1986;2:1083–1086.
- [19] Pressões EMA. Master thesis: Estudo de sinterização de cerâmicas em altas pressões; 1990.
- [20] Agatonovic R, Radojevic B, Blank V, et al. Cold sintering of copper binary systems exposed to shear deformation. *Powder Technol*. 1992;72:193–195.
- [21] Rosa AR, Gallas MR, da Jornada JAH. 'Cold' sintering of nanometric γ -Al₂O₃ at high pressures. *Ceram (Sao Paulo)*. 1996;42:162–165.
- [22] Agatonovic RM, Blank VD, Solpan Y, et al. Cold sintering of molybdenum powder under the influence of applied shear deformation. *High Temp – High Press*. 1992;24:267–270.
- [23] Costa TMH, Gallas MR, Benvenuti EV, et al. Study of nanocrystalline γ -Al₂O₃ produced by high-pressure compaction. *J Phys Chem B*. 1999;103:4278–4284.

- [24] Lashmore DS, Dariel MP, Johnson CE, et al. Restorative alloys and composites from the mixtures with acid-assisted cold sintering and formation of intermetallic compounds. U.S. 1999, 27 pp., Cont.-in-part of U.S. Ser. No. 133,316, ab.
- [25] Đuričić MR, Aćimović-Pavlović Z. Investigation of mathematical relations between technological parameters and properties of cold-sintered iron. In: Proceedings of the Advanced Science and Technology of Sintering; Kluwer Academic/Plenum Publishers, 1999; p. 565–568.
- [26] Gutmanas EY, Gotman I, Sharipova A, et al. Drug loaded biodegradable load-bearing nanocomposites for damaged bone repair. AIP Conf Proc. [2017](#);1882:020025/1–020025/11.
- [27] Yamasaki N, Yanagisawa K, Nishioka M, et al. Production of hardened boehmite by hydrothermal hot-pressing technique. Reports Res Lab Hydrothermal Chem (Kochi, Japan). [1984](#);5:48–51.
- [28] Yanagisawa K, Nishioka M, Yamasaki N. Immobilization of radioactive wastes by hydrothermal hot pressing. Am Ceram Soc Bull. [1985](#);64:1563–1567.
- [29] Yamasaki N, Nishioka M, Yanagisawa K, et al. Aggregate formation of silica under hydrothermal conditions. J Ceram Assoc Japan. [1984](#);92:150–152.
- [30] Nishizawa H. Effect of water on sintering of monoclinic ZrO₂. Yogyo Kyokai Shi/Journal Ceram Soc Japan. [1984](#);92:422–423.
- [31] Yanagisawa K, Kanahara S, Nishioka M, et al. Immobilization of radioactive wastes in hydrothermal synthetic rock. II) Hydrothermal synthesis of pollucite. J Nucl Sci Technol. [1984](#);21:558–560.
- [32] Sōmiya S. Hydrothermal reaction sintering of high density sintered oxides. Hydrothermal React Mater Sci Eng. [1989](#); 26–36.
- [33] Sōmiya S. Hydrothermal reaction sintering. Funtai Oyobi Fumatsu Yakin/Journal Japan Soc Powder Powder Metall. [1989](#);36:731–735.
- [34] Yanagisawa K, Nishioka M, Yamasaki N. Immobilization of cesium into pollucite structure by hydrothermal hot-pressing. J Nucl Sci Technol. [1987](#);24:51–60.
- [35] Yamasaki N, Yanagisawa K, Nishioka M. Solidification of inorganic powder compact by hydrothermal hot-pressing method. Yoyuen Oyobi Koon Kagaku. [1989](#);32:177–195.
- [36] Xianping M, Fukushima Y, Yanagisawa K, et al. Low temperature sintering of sepiolite by hydrothermal hot-pressing technique. Clay Sci. [1989](#);7:219–225.
- [37] Ioku K, Kai T, Nishioka M, et al. Microstructure-designed hydroxyapatite ceramics prepared by hydrothermal hot-pressing. Trans Mater Res Soc Japan. [1990](#);1:393–406.
- [38] Yanagisawa K, Nishioka M, Ioku K, et al. Neck formation of spherical silica particles by hydrothermal hot pressing. J Mater Sci Lett. [1991](#);10:7–8.
- [39] Ioku K, Kai T, Nishioka M, et al. Bioactive glass-ceramics prepared by hydrothermal hot-pressing. Nippon Kagaku Kaishi. [1991](#);1991:1408–1412.
- [40] Yamasaki N, Xiang L, Ochi H, et al. Solidification of incineration ash and arsenic-bearing waste by hydrothermal hot pressing method. Reports Res Lab Hydrothermal Chem (Kochi, Japan). [1997](#);8:65–69.
- [41] Fukushima Y, Mizutani T, Inagaki S, et al. Clay mineral-based ceramics and their manufacture. Jpn Kokai Tokkyo Koho. [1991](#); 8.
- [42] Yamasaki N, Kai T, Nishioka M, et al. Preparation of biologically active glass ceramics with rod-shaped crystals dispersion by hydrothermal hot-pressing. J Mater Sci Lett. [1992](#);11:233–234.
- [43] Nishioka M, Yamasaki N, Amano H, et al. Immobilization of tritiated water by hydrothermal hot-pressing. Waste Manag (Amsterdam Netherlands). [1992](#);12:373–378.
- [44] Meng X, Ji T, Pang W. Studies on the solidification and characterizations of USY-type molecular sieve and kaolin by hydrothermal hot-pressing technique. Gaodeng Xuexiao Huaxue Xuebao. [1993](#);14:741–744.
- [45] Kaneko M. Solidification of ion-exchange resins by hydrothermal hot-pressing. J Mater Sci Lett. [1993](#);12:591–593.
- [46] Ogawa S, Minami S. Reuse technology of sewage sludge. Ueisuto, Risosu. [1993](#);27:2–10.
- [47] Yanagisawa K, Sasaki M, Nishioka M, et al. Preparation of sintered compacts of anatase by hydrothermal hot-pressing. J Mater Sci Lett. [1994](#);13:765–766.
- [48] Gamoh K, Yamasaki N. Dehydration condensation of amino acids under hydrothermal hot-pressing environments. Bunseki Kagaku. [1998](#);47:303–308.
- [49] Onoki T, Hosoi K, Hashida T. Joining hydroxyapatite ceramics and titanium alloys by hydrothermal method. Key Eng Mater. [2003](#);240–242:571–574.
- [50] Onoki T, Hosoi K, Hashida T. Novel techniques of hydroxyapatite coating on titanium utilizing hydrothermal hot-pressing. Trans Mater Res Soc Japan. [2004](#);29:2675–2678.
- [51] Yokosawa K, Korablov S, Tohji K, et al. The possibility of diamond sintering by hydrothermal hot-pressing. AIP Conf Proc. [2006](#);833:100–103.
- [52] Katsuyama S, Kishida A, Ito M. Synthesis of Na₂Co₂O₄ by the hydrothermal hot-pressing and its thermoelectric properties. J Alloys Compd. [2006](#);414:215–220.
- [53] Nakahira A, Takimura M, Yamasaki Y. Synthesis of bulky mesoporous silica (FSM) by hydrothermal hot-pressing method. J Non Cryst Solids. [2007](#);353:4203–4207.
- [54] Zhu L, Lian G, Tan M, et al. Reaction of hexagonal boron nitride nanocrystals under mild hydrothermal conditions. Zeitschrift Fuer Naturforschung, B Chem Sci. [2008](#);63:742–746.
- [55] Liu X, Cui D, Li Y, et al. Preparation and characterization of ZrO₂ porous nanosolid and its composite fluorescent materials. J Mater Sci. [2008](#);43:1730–1733.
- [56] Kubo T, Takeuchi M, Matsuoka M, et al. Morphologic control of Pt supported titanate nanotubes and their photocatalytic property. Catal Letters. [2009](#);130:28–36.
- [57] Liu X. Preparation of γ-Al₂O₃ porous nanosolid/fluorescein fluorescent nanocomposites by a simple method. Mater Sci Eng B Adv Funct Solid-State Mater. [2010](#);175:86–89.
- [58] Nakahira A, Kubo T, Yamasaki Y. Microstructural control of mesoporous bulk composed of TiO₂-derived titanate nanotubes. ACS Appl Mater Interfaces. [2010](#);2:1136–1140.
- [59] Xie Y, Li J, Yue F, et al. Grain size effect and low temperature-sintering technologies for dielectric nanoceramics. Guisuanyan Xuebao. [2012](#);40:872–878.
- [60] Onoda H, Yamasaki T. Synthesis of bulk rare earth phosphates UV hydrothermal hot pressing and their properties. Kidorui. [2013](#);62:78–79.

- [61] Baker A, Guo H, Guo J, et al. Utilizing the cold sintering process for flexible-printable electroceramic device fabrication. *J Am Ceram Soc.* **2016**;99:3202–3204.
- [62] Guo H, Baker A, Guo J, et al. Protocol for ultralow-temperature ceramic sintering: an integration of nanotechnology and the cold sintering process. *ACS Nano.* **2016**;10:10606–10614.
- [63] Guo J, Guo H, Baker AL, et al. Cold sintering: a paradigm shift for processing and integration of ceramics. *Angew Chemie – Int Ed.* **2016**;55:11457–11461.
- [64] Guo J, Berbano SS, Guo H, et al. Cold sintering process of composites: bridging the processing temperature gap of ceramic and polymer materials. *Adv Funct Mater.* **2016**;26:7115–7121.
- [65] Bouville F, Studart AR. Geologically-inspired strong bulk ceramics made with water at room temperature. *Nat Commun.* **2017**;8:14655.
- [66] Guo J, Baker AL, Guo H, et al. Cold sintering process: a new era for ceramic packaging and microwave device development. *J Am Ceram Soc.* **2017**;100:669–677.
- [67] Berbano SS, Guo J, Guo H, et al. Cold sintering process of $\text{Li}_{1.5}\text{Al}_{0.5}\text{Ge}_{1.5}(\text{PO}_4)_3$ solid electrolyte. *J Am Ceram Soc.* **2017**;100:2123–2135.
- [68] Funahashi S, Guo H, Guo J, et al. Cold sintering and co-firing of a multilayer device with thermoelectric materials. *J Am Ceram Soc.* **2017**;100:3488–3496.
- [69] Väättäjä M, Kähäri H, Ohenoja K, et al. 3D printed dielectric ceramic without a sintering stage. *Sci Rep.* **2018**;8:15955.
- [70] Miao Y, Du P, Wang Z, et al. Ultrasonic vibration imposed on nanoparticle-based ZnO film improves the performance of the ensuing perovskite solar cell. *Mater Res Express.* **2018**;5:026404/1–026404/10.
- [71] Bang SH, De Beauvoir TH, Randall CA. Densification of thermodynamically unstable tin monoxide using cold sintering process. *J Eur Ceram Soc.* **2019**;39:1230–1236.
- [72] Nayir S, Waryoba DR, Rajagopalan R, et al. Cold sintering of a covalently bonded MoS_2 /graphite composite as a high capacity Li-ion electrode. *Chem Nano Mat.* **2018**;4:1088–1094.
- [73] Guo J, Legum B, Anasori B, et al. Cold sintered ceramic nanocomposites of 2D MXene and zinc oxide. *Adv Mater (Weinheim. Ger).* **2018**;30, n/a.
- [74] Taveri G, Grasso S, Gucci F, et al. Bio-inspired hydro-pressure consolidation of silica. *Adv Funct Mater.* **2018**;28, n/a.
- [75] Yamasaki N, Yanagisawa K, Nishioka M, et al. A hydrothermal hot-pressing method: apparatus and application. *J Mater Sci Lett.* **1986**;5:355–356.
- [76] Riman IRE, Mead B, Examiner P, et al. Phase sintering of Ceramc Ee 7386 E. US Pat. 8,313,802 2012.
- [77] Randall CA, Guo J, Baker A, et al. Cold sintering ceramics and composites. U.S. Pat. Appl. Publ. 2017, 24 pp., Cont. of Appl. No. PCT/US2016/053772.
- [78] Gutmanas EY. Design of alloys and materials using cold sintering. In *Proceedings of the Modern Developments in Powder Metallurgy*; 1985.
- [79] Sun P, Wu HC. Splitting tensile strength of fly ash activated by hydrothermal hot-pressing process. *J Mater Civ Eng.* **2009**;21:356–361.
- [80] Yanagisawa K, Ioku K, Yamasaki N. Crystallization of amorphous hydrous titania under hydrothermal hot-pressing conditions. *Nippon Seramikkusu Kyokai Gakujutsu Ronbunshi/Journal Ceram Soc Japan.* **1994**;102:1091–1093.
- [81] Baker A, Guo H, Guo J, et al. Utilizing the cold sintering process for flexible-printable electroceramic device fabrication. *J Am Ceram Soc.* **2016**;99:3202–3204.
- [82] Toraya H, Yoshimura M, Somiya S. Hydrothermal reaction-sintering of monoclinic HfO_2 . *J Am Ceram Soc.* **1982**;65:c159–c160.
- [83] Vakifahmetoglu C, Anger JF, Atakan V, et al. Reactive hydrothermal liquid-phase densification (rHLPD) of ceramics – a study of the $\text{BaTiO}_3[\text{TiO}_2]$ composite system. *J Am Ceram Soc.* **2016**;99:3893–3901.
- [84] Schiedt VU, Reinwein H. Zur Infrarot-Spektroskopie von Aminosäuren I. Mitt.: Eine neue Präparationstechnik zur Infrarot-Spektroskopie von Aminosäuren und anderen polaren Verbindungen. *Zeitschrift für Naturforschung B.* **1952**;7:270–277.
- [85] Stimson MM, O'Donnell MJ. The infrared and ultraviolet absorption spectra of cytosine and isocytosine in the solid state. *J Am Chem Soc.* **1952**;74:1805–1808.
- [86] Gotman I, Gutmanas EY. Joining of P/M high speed tool steel with cobalt and ferrous alloys by high pressure consolidation. In *Proc Horiz Powder Metall Proc Int Powder Metall Conf Exhib*; Schmid, 1986; Vol. 2, pp. 703–706.
- [87] Gutmanas EY, Goldman DB, Hart S, et al. Cold sintered 4640 Steel-vanadium carbide composites. In *Proc Powder Metall Int*; Schmid. **1986**;2:1083–1086.
- [88] Gutmanas EY, Zak D. Mechanical behavior of cold-sintered high-speed steel-carbides composites. *Mod Dev Powder Metall.* **1988**;20:421–429.
- [89] Dariel MP, Ratzker M, Eichmiller FC. Acid-assisted consolidation of powder compacts: cold-welding or cold sintering. *J Mater Sci.* **1999**;34:2601–2607.
- [90] Glenn L. Beane PM 'cold forming' process eliminates sintering. *Met Powder Rep.* **1996**;51:5.
- [91] Roy DM, Gouda GR. Porosity-strength relation in cementitious materials with very high Strengths. *J Am Ceram Soc.* **1973**;56:549–550.
- [92] Sōmiya S, Hirano S, Yoshimura M, et al. Hydrothermal reaction sintering of Cr_2O_3 and iron oxides. In *Proceedings of the Hydrothermal Reactions for Materials Science and Engineering*; Gakujutsu Bunken Fukyu-kai, 1989; p. 4–14.
- [93] Yamasaki N, Yanagisawa K, Feng Q. Hydrothermal process. *Seramikkusu.* **1999**;34:377–382.
- [94] Medri V, Servadei F, Bondoni R, et al. Nano-to-macroporous TiO_2 (anatase) by cold sintering process. *J Eur Ceram Soc.* **2019**;39:2453–2462.
- [95] Nishizawa H, Tebika H, Yamasaki N. Fabrication of stabilized zirconia compressed body under hydrothermal conditions and its sintering. *Yogyo Kyokaishi.* **1984**;92:420–421.
- [96] Ndayishimiye A, Largeteau A, Prakasam M, et al. Low temperature hydrothermal sintering process for the quasi-complete densification of nanometric α -quartz. *Scr Mater.* **2018**;145:118–121.
- [97] Ndayishimiye A, Largeteau A, Mornet S, et al. Hydrothermal sintering for densification of silica. Evidence for the role of water. *J Eur Ceram Soc.* **2018**;38:1860–1870.
- [98] Costa TMHH, Gallas MR, Benvenuti EV, et al. Infrared and thermogravimetric study of high pressure consolidation in alkoxide silica gel powders. *J Non Cryst Solids.* **1997**;220:195–201.
- [99] Katsuyama S, Takiguchi Y, Ito M. Synthesis of $\text{Ca}_3\text{Co}_4\text{O}_9$ ceramics by polymerized complex and hydrothermal hot-pressing processes and

- investigation of its thermoelectric properties. *Int Conf Thermoelectr ICT Proc.* **2007**;43:103–107.
- [100] Onoda H, Yamasaki T. Synthesis of bulk lanthanum polyphosphate and other rare earth phosphates through hydrothermal hot-pressing. *J Adv Ceram.* **2013**;2:301–307.
- [101] Nishioka M, Yamasaki N, Amano H, et al. Immobilization of tritiated water by hydrothermal hot-pressing. *Waste Manag.* **1992**;12:373–378.
- [102] Nishioka M, Yamasaki N. Immobilization of cesium into pollucite structure by hydrothermal hot-pressing. *J Nucl Sci Technol.* **1987**;24:51–60.
- [103] Ioku K, Yamamoto K, Yanagisawa K, et al. Low temperature sintering of hydroxyapatite by hydrothermal Hot-pressing. *Phosphorus Res Bull.* **1994**;4:65–70.
- [104] Khelifi O, Kozuki Y, Murakami H, et al. Development of a new porous carrier for ammonium removal as innovative uses for waste materials. *J Solid Waste Technol Manag.* **2003**;29:118–126.
- [105] Nakahira A, Takezoe S, Yamasaki Y. Synthesis of dense Y-zeolite bulks with large surface area using a hydrothermal hot-pressing (HHP) process. *Chem Lett.* **2004**;33:1400–1401.
- [106] Takimura M, Nagata H, Yamasaki Y, et al. Synthesis and characterization of bulky FSM with interconnected mesopore-networks using an HHP method. *J Ceram Soc Japan.* **2006**;114:554–557.
- [107] Nagata H, Hirao N, Onoki T, et al. Synthesis and characterization of bulky mesoporous silica Pd-MCM-41. *J Ceram Soc Japan.* **2008**;116:216–219.
- [108] Luukkonen T, Abdollahnejad Z, Yliniemi J, et al. One-part alkali-activated materials: a review. *Cem Concr Res.* **2018**;103:21–34.
- [109] Yamasaki N. Development of recycling technologies, and functional material formation by hydrothermal processes. *J Ceram Soc Japan.* **2003**;111:709–715.
- [110] Nishioka M, Yanagisawa K, Yamasaki N. Solidification of sludge ash by hydrothermal hot-pressing. *Res J Water Pollut Control Fed.* **1991**;62:926–932.
- [111] Nishioka M, Yamasaki N. Fundamental study of the recycling of sludge ash by a hydrothermal reaction. *Ueisuto Risosu.* **1993**;27:11–15.
- [112] Veloza ZM, Yanagizawa K, Yamasaki N. Recycling waste glasses by means of the hydrothermal hot pressing method. *J Mater Sci Lett.* **1999**;18:1811–1813.
- [113] Yanagisawa K, Matamoros-Veloza Z, Rendón-Angeles JC, et al. Novel route for recycling of steel-making slag by means of the hydrothermal hot-pressing method. *J Mater Sci Lett.* **2002**;21:693–695.
- [114] Hirai N, Maeda S, Katsuyama S, et al. Fabrication of porous solidified materials from blast furnace slag using hydrothermal hot-pressing method and measurement of thermal conductivity of solidified materials. *Tetsu to Hagane.* **2009**;95:1–6.
- [115] Matamoros-Veloza Z, Rendón-Angeles JC, Yanagisawa K, et al. Preparation of foamed glasses from CRT TV glass by means of hydrothermal hot-pressing technique. *J Eur Ceram Soc.* **2008**;28:739–745.
- [116] Xue F, Song H, Ji Y, et al. Hydrothermal hot-pressing solidification of coal fly ash and its ability of fixing heavy metal. *J Residuals Sci Technol.* **2015**;12:143–148.
- [117] Song H, Wei L, Ji Y, et al. High-strength solidification of fly ash/carbide slag and its fixing ability for heavy metals. *J Residuals Sci Technol.* **2017**;14:155–160.
- [118] Matamoros-Veloza Z, Yanagisawa K, Rendón-Angeles JC, et al. Preparation of porous materials from hydrothermally hot pressed glass compacts. *J Mater Sci Lett.* **2002**;21:1855–1858.
- [119] Matamoros-Veloza Z, Yanagisawa K, Rendón-Angeles JC, et al. The effect of hydrothermal hot-pressing parameters on the fabrication of porous ceramics using waste glass. *J Phys Condens Matter.* **2004**;16:S1361–S1372.
- [120] Yamasaki N, Yamasaki Y, Tohji K, et al. Hydrothermal dynamics on environmental problems using the aspect of earth science. *J Mater Sci.* **2006**;41:1599–1604.
- [121] Onoki T, Tanaka M, Hashida T. New processing method for hydroxyapatite coating by hydrothermal techniques. *Funtai Oyobi Funmatsu Yakin.* **2005**;52:861–864.
- [122] Li JG, Hashida T. In situ formation of hydroxyapatite-whisker ceramics by hydrothermal hot-pressing method. *J Am Ceram Soc.* **2006**;89:3544–3546.
- [123] Ishihara S, Matsumoto T, Onoki T, et al. New concept bioceramics composed of octacalcium phosphate (OCP) and dicarboxylic acid-intercalated OCP via hydrothermal hot-pressing. *Mater Sci Eng C.* **2009**;29:1885–1888.
- [124] Onoki T, Nakahira A, Tago T, et al. Novel low temperature processing techniques for apatite ceramics and chitosan polymer composite bulk materials and its mechanical properties. *Appl Surf Sci.* **2012**;262:263–266.
- [125] Irie A, Ohno J, Hayakawa T, et al. Transparent film formation of DNA/cationic polymer complexes by hydrothermal hot pressing: observation of cell culture on films and biodegradation of films in vivo. *J Hard Tissue Biol.* **2013**;22:105–114.
- [126] Udawatte CP, Yanagisawa K, Kamakura T, et al. Solidification of xonotlite fibers with chitosan by hydrothermal hot pressing. *Mater Lett.* **2000**;45:298–301.
- [127] Udawatte CP, Yanagisawa K, Kamakura T, et al. Hardening of hydrothermal hot pressed calcium silicate compacts with rice husk as fiber reinforcement. *Mater Res Innov.* **2000**;3:297–301.
- [128] Sun P, Wu HC. Transition from brittle to ductile behavior of fly ash using PVA fibers. *Cem Concr Compos.* **2008**;30:29–36.
- [129] Liu X. Preparation of γ - Al_2O_3 porous nanosolid/fluorescein fluorescent nanocomposites by a simple method. *Mater Sci Eng B Solid-State Mater Adv Technol.* **2010**;175:86–89.
- [130] Xie Y, Yin S, Yamane H, et al. Low temperature sintering and color of a new compound $\text{Sn}_{1.24}\text{Ti}_{1.94}\text{O}_{3.66}(\text{OH})_{1.50}\text{F}_{1.42}$. *Solid State Sci.* **2009**;11:1703–1708.
- [131] Kubo T, Nakahira A, Yamasaki Y. Fabrication of mesoporous bulk composed of titanate nanotubes by hydrothermal hot-pressing technique. *J Mater Res.* **2007**;22:1286–1291.
- [132] Nelo M, Peräntie J, Siponkoski T, et al. Upside-down composites: electroceramics without sintering. *Appl Mater Today.* **2019**;15:83–86.
- [133] Kähäri H, Teirikangas M, Juuti J, et al. Improvements and modifications to room-temperature fabrication method for dielectric Li_2MoO_4 ceramics. *J Am Ceram Soc.* **2015**;98:687–689.
- [134] Jiang A, Ke D, Xu L, et al. Cold hydrostatic sintering: from shaping to 3D printing. *J Materiomics.* **2019**;5:496–501.

- [135] Guo H, Baker A, Guo J, et al. Cold sintering process: a novel technique for low-temperature ceramic processing of ferroelectrics. *J Am Ceram Soc.* **2016**;99:3489–3507.
- [136] Maria JP, Kang X, Floyd RD, et al. Cold sintering: current status and prospects. *J Mater Res.* **2017**;32:3205–3218.
- [137] Zhao Y, Berbano SS, Gao L, et al. Cold-sintered V_2O_5 -PEDOT:PSS nanocomposites for negative temperature coefficient materials. *J Eur Ceram Soc.* **2019**;39:1257–1262.
- [138] Ma J, Li H, Wang H, et al. Composition, microstructure and electrical properties of $K_{0.5}Na_{0.5}NbO_3$ ceramics fabricated by cold sintering assisted sintering. *J Eur Ceram Soc.* **2019**;39:986–993.
- [139] Huang HQ, Tang J, Liu J. Preparation of $Na_{0.5}Bi_{0.5}TiO_3$ ceramics by hydrothermal-assisted cold sintering. *Ceram Int.* **2019**;45:6753–6758.
- [140] Wang D, Zhou D, Zhang S, et al. Cold-sintered temperature stable $Na_{0.5}Bi_{0.5}MoO_4$ - Li_2MoO_4 microwave composite ceramics. *ACS Sustain Chem Eng.* **2018**;6:2438–2444.
- [141] Guo J, Pfeifferberger N, Beese A, et al. Cold sintering $Na_2Mo_2O_7$ ceramic with poly(ether imide) (PEI) polymer to realize high-performance composites and integrated multilayer circuits. *ACS Appl Nano Mater.* **2018**;1:3837–3844.
- [142] Induja IJ, Sebastian MT. Microwave dielectric properties of mineral sillimanite obtained by conventional and cold sintering process. *J Eur Ceram Soc.* **2017**;37:2143–2147.
- [143] Hong WB, Li L, Cao M, et al. Plastic deformation and effects of water in room-temperature cold sintering of NaCl microwave dielectric ceramics. *J Am Ceram Soc.* **2018**;101:4038–4043.
- [144] Li L, Hong WB, Yang S, et al. Effects of water content during cold sintering process of NaCl ceramics. *J Alloys Compd.* **2019**;787:352–357.
- [145] Induja IJ, Sebastian MT. Microwave dielectric properties of cold sintered Al_2O_3 -NaCl composite. *Mater Lett.* **2018**;211:55–57.
- [146] Liu Y, Liu P, Hu C. Low-temperature preparation and microwave dielectric properties of cold sintered $Li_2Mg_3TiO_6$ nanocrystalline ceramics. *Ceram Int.* **2018**;44:21047–21052.
- [147] Kang X, Floyd R, Lowum S, et al. Cold sintering with dimethyl sulfoxide solutions for metal oxides. *J Mater Sci.* **2019**;54:7438–7446.
- [148] Zhao X, Guo J, Wang K, et al. Introducing a ZnO-PTFE (polymer) nanocomposite varistor via the cold sintering process. *Adv Eng Mater.* **2018**;20, n/a.
- [149] Jing Y, Luo N, Wu S, et al. Remarkably improved electrical conductivity of ZnO ceramics by cold sintering and post-heat-treatment. *Ceram Int.* **2018**;44:20570–20574.
- [150] Nie J, Zhang Y, Chan JM, et al. Water-assisted flash sintering: flashing ZnO at room temperature to achieve ~98% density in seconds. *Scr Mater.* **2018**;142:79–82.
- [151] Lowum S, Floyd R, Bermejo R, et al. Mechanical strength of cold-sintered zinc oxide under biaxial bending. *J Mater Sci.* **2019**;54:4518–4522.
- [152] Guo J, Guo H, Heidary DSB, et al. Semiconducting properties of cold sintered V_2O_5 ceramics and co-sintered V_2O_5 -PEDOT:PSS composites. *J Eur Ceram Soc.* **2017**;37:1529–1534.
- [153] Nakaya H, Iwasaki M, de Beauvoir TH, et al. Applying cold sintering process to a proton electrolyte material: CsH_2PO_4 . *J Eur Ceram Soc.* **2019**;39:396–401.
- [154] Liu Y, Sun Q, Wang D, et al. Development of the cold sintering process and its application in solid-state lithium batteries. *J Power Sources.* **2018**;393:193–203.
- [155] Lee W, Lyon CK, Seo J-H, et al. Ceramic-Salt composite electrolytes from cold sintering. *Adv Funct Mater.* **2019**;29:1807872.
- [156] Pereira da Silva JG, Bram M, Laptev AM, et al. Sintering of a sodium-based NASICON electrolyte: a comparative study between cold, field assisted and conventional sintering methods. *J Eur Ceram Soc.* **2019**;39:2697–2702.
- [157] Leng H, Huang J, Nie J, et al. Cold sintering and ionic conductivities of $Na_{3.256}Mg_{0.128}Zr_{1.872}Si_2PO_{12}$ solid electrolytes. *J Power Sources.* **2018**;391:170–179.
- [158] Liu Y, Liu J, Sun Q, et al. Insight into the microstructure and ionic conductivity of cold sintered NASICON solid electrolyte for solid-state batteries. *ACS Appl Mater Interfaces.* **2019**;11:27890–27896.
- [159] Berbano SS, Guo J, Guo H, et al. Cold sintering process of $Li_{1.5}Al_{0.5}Ge_{1.5}(PO_4)_3$ solid electrolyte. *J Am Ceram Soc.* **2017**;100:2123–2135.
- [160] Seo JH, Guo J, Guo H, et al. Cold sintering of a Li-ion cathode: $LiFePO_4$ -composite with high volumetric capacity. *Ceram Int.* **2017**;43:15370–15374.
- [161] Seo J-HH, Verlinde K, Guo J, et al. Cold sintering approach to fabrication of high rate performance binderless $LiFePO_4$ cathode with high volumetric capacity. *Scr Mater.* **2018**;146:267–271.
- [162] Heidary DSB, Guo J, Seo JH, et al. Microstructures and electrical properties of V_2O_5 and carbon-nanofiber composites fabricated by cold sintering process. *Jpn J Appl Phys.* **2018**;57:025702/1–025702/6.
- [163] Pearson RG. Hard and soft acids and bases. *J Am Chem Soc.* **1963**;85:3533–3539.
- [164] Pearson RG. Recent advances in the concept of hard and soft acids and bases. *J Chem Educ.* **1987**;64:561.
- [165] Lee LH. Applications of the hard-soft acid-base (HSAB) principle to solid adhesion and surface tribointeractions. In *Surfactants and macromolecules: self-assembly at interfaces and in bulk.* 2008.
- [166] Lee L-H. Hard-soft acid-base (HSAB) principle for solid adhesion and surface interactions. In *Fundamentals of adhesion.* New York; **2013**.
- [167] Slack JMW. Molecular biology of the cell. Principles of tissue engineering; **2014**. p. 127–145.
- [168] Schmuckler JS. Solubility product constant, Ksp. *J Chem Educ.* **2009**.
- [169] Pichtel J. Solubility product constants at 25 °C. *Waste Manag Prac.* **2014**; 631–634.
- [170] Wagle DV, Baker GA. Cold welding: a phenomenon for spontaneous self-healing and shape genesis at the nanoscale. *Mater Horizons.* **2015**;2:157–167.
- [171] Mehrer H. Diffusion in solids. Springer Ser Solid-State Sci. **2007**. Available from: <https://www.springer.com/gp/book/9783540714866>
- [172] Takigawa R, Higurashi E, Asano T. Room-temperature wafer bonding of $LiNbO_3$ and SiO_2 using a modified surface activated bonding method. *Jpn J Appl Phys.* **2018**;57:06HJ12.
- [173] Ebneshajjad S. Handbook of adhesives and surface preparation. Oxford: Elsevier; **2011**.

- [174] Grasso S, Tsujii N, Jiang Q, et al. Ultra low thermal conductivity of disordered layered p-type bismuth telluride. *J Mater Chem C*. 2013;1:2362–2367.
- [175] Gutmanas EY, Lawley A. Cold sintering - a new powder consolidation process. *Prog Powder Metall*. 1984;39, Technical report.
- [176] Park S, Han HN, Oh KH, et al. Model for compaction of metal powders. *Int J Mech Sci*. 1999;41:121–144.
- [177] Lee DN, Kim HS. Plastic yield behaviour of porous metals. *Powder Metall*. 1992;35:275–279.
- [178] Govindarajan RM, Aravas N. Deformation processing of metal powders: part I – cold isostatic pressing. *Int J Mech Sci*. 2003;36:343–357.
- [179] Panelli R, Filho FA. Compaction equation and its use to describe powder consolidation behavior. *Powder Metall*. 1998;41:131–133.
- [180] Ponraj NV, Azhagurajan A, Vettivel SC. Microstructure, consolidation and mechanical behaviour of Mg/n-TiC composite. *Alexandria Eng J*. 2016;55:2077–2086.
- [181] Panelli R, Filho FA. A study of a new phenomenological compacting equation. *Powder Technol*. 2001;114:255–261.
- [182] Kawakita K. Some Considerations on powder compression equations. *Powder Technol*. 1969;4:61–68.
- [183] Franssen R. Rheology of synthetic rocksalt: with emphasis on the influence of deformation history and geometry on the flow behaviour; [Faculteit Aardwetenschappen der Universiteit Utrecht], 1993; Vol. 113; ISBN 9071577678.
- [184] Schenk O, Urai JL. Microstructural evolution and grain boundary structure during static recrystallization in synthetic polycrystals of sodium chloride containing saturated brine. *Contrib to Mineral Petrol*. 2004;146:671–682.
- [185] Educational poster «Solubility table» – solubility of electrolytes in aqueous solutions.
- [186] Warren JK. *Evaporites a geological compendium*; 2016; ISBN 9783319135113.
- [187] Dean JA. *Lange's handbook of chemistry*. London; 1998.
- [188] Prévost M, Oliveira IT, Kocher JP, et al. Free energy of cavity formation in liquid water and hexane. *J Phys Chem*. 1996;100:2738–2743.
- [189] Pagni R. Modern physical organic chemistry (Eric V. Anslyn and Dennis A. Dougherty). *J Chem Educ*. 2006;83:387.
- [190] July P. Química Nova review of the synthesis of layered double hydroxides: a thermodynamic approach. *Quim Nova*. 2015;2:1–21.
- [191] Cameron FK, Robinson WO. The solubility of calcium carbonate in aqueous solutions of potassium chloride and potassium Sulphate at 25 °. *J Phys Chem*. 2005;11:577–580.
- [192] Frear GL, Johnston J. The solubility of calcium carbonate (calcite) in certain aqueous solutions at 25 ° 1. *J Am Chem Soc*. 1929;51:2082–2093.
- [193] Morey GW, Fournier RO, Rowe JJ. The solubility of amorphous silica at 25 deg C. *J Geophys Res*. 1997;102:1995–2002.
- [194] Wood JA. The solubility of quartz in water at high temperatures and pressures. *Am J Sci*. 2010;256:40–47.
- [195] King E. J. the solubility of silica. *Lancet*. 1938;231:1236–1238.
- [196] Weng L, Sagoe-Crentsil K, Weng L. Dissolution processes, hydrolysis and condensation reactions during geopolymer synthesis: part I-Low Si/Al ratio systems. *J Mater Sci*. 2007;42:2997–3006.
- [197] Anderson GM, Burnham CW. The solubility of quartz in super-critical water. *Am J Sci*. 1965;263:494–511.
- [198] Fournier RO, Potter RW. An equation correlating the solubility of quartz in water from 25 ° to 900 °C at pressures up to 10,000 bars. *Geochim Cosmochim Acta*. 1982;46:1969–1973.
- [199] Young JA. Sodium chloride; 2009; 84.
- [200] Sole MJ. Hydrolysis of sodium chloride. *Trans Faraday Soc*. 1970;66:3065–3074.
- [201] Reynolds DA, Herting DL. Solubilities of sodium nitrate, sodium nitrite, and sodium aluminate in simulated nuclear waste. 1984.
- [202] American elements safety data sheet – tungsten nanoparticles; 2015.
- [203] Lillard RS. The nature of oxide films on tungsten in acidic and alkaline solutions. *J Electrochem Soc*. 2006;145:2718.
- [204] Funahashi S, Guo J, Guo H, et al. Demonstration of the cold sintering process study for the densification and grain growth of ZnO ceramics. *J Am Ceram Soc*. 2017;100:546–553.
- [205] Eixenberger JE, Anders CB, Hermann RJ, et al. Rapid dissolution of ZnO nanoparticles induced by biological buffers significantly impacts cytotoxicity. *Chem Res Toxicol*. 2017;30:1641–1651.
- [206] Reed RB, Ladner DA, Higgins CP, et al. Solubility of nano-zinc oxide in environmentally and biologically important matrices. *Environ Toxicol Chem*. 2012;31:93–99.
- [207] Bauer G, Güther V, Hess H, et al. Vanadium and vanadium compounds. *Ullmann's Encycl Ind Chem*. 2017: 1–22. DOI:10.1002/14356007.a27_367.pub2
- [208] Bell RC, Castleman AW, Thorn DL. Vanadium oxide complexes in room-temperature chloroaluminate molten salts. *Inorg Chem*. 1999;38:5709–5715.
- [209] Costigan M, Cary R, Dobson S. Vanadium pentoxide and other inorganic vanadium compounds. *World Health Organization*; 2001.
- [210] Bruyère VIE, Morando PJ, Blesa MA. The dissolution of vanadium pentoxide in aqueous solutions of oxalic and mineral acids. *J Colloid Interface Sci*. 1999;209:207–214.
- [211] Skyllas-Kazacos M, Limantari Y. Kinetics of the chemical dissolution of vanadium pentoxide in acidic bromide solutions. *J Appl Electrochem*. 2004;34:681–685.
- [212] Fedoročková A, Raschman P. Effects of pH and acid anions on the dissolution kinetics of MgO. *Chem Eng J*. 2008;143:265–272.
- [213] Aphane ME. The hydration of magnesium oxide with different reactivities by water and magnesium acetate, 2007.
- [214] Macdonald DD, Owen D. The dissolution of magnesium oxide in dilute sulfuric acid. *Can J Chem*. 1971;49:3375–3380.
- [215] Prajapati RR, Srinivasan TG, Chandramouli V, et al. Dissolution kinetics of zirconium dioxide in nitric acid. *Desalin Water Treat*. 2014;52:490–497.
- [216] Yoshimura M, Hiuga T, Somiya S. Dissolution and reaction of yttria-stabilized zirconia single crystals in hydrothermal solutions. *J Am Ceram Soc*. 1986;69:583–584.
- [217] Rosenthal SB. Changing the wetting properties of titanium dioxide surfaces with visible and near infrared light, 2016.

- [218] Lisoni JG, Lei CH, Hoffmann T, et al. Hydrothermal growth of BaTiO₃ on TiO₂ single crystals. *Surf Sci.* **2002**;515:431–440.
- [219] Glebov VA. Effect of ligands on the hydration shell of titanium ions. *J Struct Chem.* **1971**;11:750–754.
- [220] Pfaff G. BaTiO₃ preparation by reaction of TiO₂ with Ba(OH)₂. *J Eur Ceram Soc.* **1991**;8:35–39.
- [221] Dadze TP, Kashirtseva GA, Novikov MP, et al. Solubility of MoO₃ in acid solutions and vapor-liquid distribution of molybdic acid. *Fluid Phase Equilib.* **2017**;440:64–76.
- [222] Rempel KU, Williams-Jones AE, Migdisov AA. The solubility of molybdenum dioxide and trioxide in HCl-bearing water vapour at 350 °C and pressures up to 160 bars. *Geochim Cosmochim Acta.* **2008**;72:3074–3083.
- [223] Rempel KU, Migdisov AA, Williams-Jones AE. The solubility and speciation of molybdenum in water vapour at elevated temperatures and pressures: Implications for ore genesis. *Geochim Cosmochim Acta.* **2006**;70:687–696.
- [224] Separation M. Membranes and membrane separation processes. *Ullmann's Encycl Ind Chem.* **2000**;16:1–83.
- [225] Hurtig NC, Williams-Jones AE. An experimental study of the solubility of MoO₃ in aqueous vapour and low to intermediate density supercritical fluids. *Geochim Cosmochim Acta.* **2014**;136:169–193.
- [226] Barinova OP, Ermochenkova IM, Kuchuk ZS, et al. Growth of Li₂MoO₄ crystals from activated water solutions. *Glas Ceram (English Transl Steklo i Keramika).* **2016**;72:425–429.
- [227] Kyarov AA, Karov ZG, Khochuev IY, et al. Solubility and physicochemical properties of lithium molybdate-n-butanol-water solutions at 25 °C. *Russ J Inorg Chem.* **2007**;52:455–459.
- [228] Willey JD. The effect of pressure on the solubility of minerals in seawater at 0 °C. *Mar Chem.* **1974**;2:239–250.
- [229] Railsback LB. Railsback – an earth scientists periodic table of the elements and their ions. *Geol Soc Am.* **2012**;31:2012.
- [230] Richens DT. The chemistry of aqua ions. Chichester; **1997**.
- [231] Glasser L, Jones F. Systematic thermodynamics of hydration (and of solvation) of inorganic solids. *Inorg Chem.* **2009**;48:1661–1665.
- [232] Moldoveanu SC, David V. Mobile phases and their properties. *Essentials Mod HPLC Sep.* **2012**; 363–447.
- [233] Archer DG, Wang P. The dielectric constant of water and Debye Hückel limiting law slopes. *J Phys Chem Ref Data.* **1990**;19:371–411.
- [234] Takeuchi T, Kawamura K. Effect of the crystal structure on the acid dissolution of zirconium oxide. *Trans Japan Inst Met.* **2014**;13:262–264.
- [235] James WJ, Custeho WG, Stwumanis ME. Dissolution rates, electrochemical and passivation properties of alpha Zr-O solid solutions. *Corros Sci.* **1962**;2:237–254.
- [236] Haynes WM. CRC handbook of chemistry and physics. 96th ed. Boca Raton: CRC Press; **2015**.
- [237] Hong WB, Li L, Yan H, et al. Cold sintering and microwave dielectric properties of dense HBO₂-II ceramics. *J Am Ceram Soc.* **2019**;102:5934–5940.
- [238] Li M, Lin D, Zhu L. Effects of water chemistry on the dissolution of ZnO nanoparticles and their toxicity to *Escherichia coli*. *Environ Pollut.* **2013**;173:97–102.
- [239] David C, Cruz-Gonzalez S, Salvador J, et al. Thermodynamics and kinetics of the dissolution of ZnO nanoparticles followed by AGNES. *J Phys Chem C.* **2012**;116:11758–11767.
- [240] Chu KR, Lee E, Jeong SH, et al. Effect of particle size on the dissolution behaviors of poorly water-soluble drugs. *Arch Pharm Res.* **2012**;35:1187–1195.
- [241] Mosharrar M, Nyström C. The effect of particle size and shape on the surface specific dissolution rate of micro-sized practically insoluble drugs. *Int J Pharm.* **1995**;122:35–47.
- [242] Sun J, Wang F, Sui Y, et al. Effect of particle size on solubility, dissolution rate, and oral bioavailability: evaluation using coenzyme Q10 as naked nanocrystals. *Int J Nanomedicine.* **2012**;7:5733–5744.
- [243] Lee WE. Ceramic processing and sintering. New York (NY): Marcel Dekker; **2012**; Vol. 41.
- [244] Hosoi K, Kawai S, Yanagisawa K, et al. Densification process for spherical glass powders with the same particle size by hydrothermal hot pressing. *J Mater Sci.* **1991**;26:6448–6452.
- [245] Gonzalez-Julian J, Neuhaus K, Bernemann M, et al. Unveiling the mechanisms of cold sintering of ZnO at 250 °C by varying applied stress and characterizing grain boundaries by Kelvin probe force microscopy. *Acta Mater.* **2018**;144:116–128.
- [246] Biesuz M, Taveri G, Duff AI, et al. A theoretical analysis of cold sintering. *Adv Appl Ceram.* **2019**;119:75–89.
- [247] Gibson RE. General considerations of the effect of pressure on solubility. *Eos, Trans Am Geophys Union.* **1938**;19:273–274.
- [248] Bateman LA, Fernelius WC. Demonstration of a negative temperature coefficient of solubility. *J Cem Educ.* **1944**; 315.
- [249] Sengul MY, Guo J, Randall CA, et al. Water-mediated surface diffusion mechanism enables the cold sintering process: a combined computational and experimental study. *Angew Chemie Int Ed.* **2019**;131:12550–12554.
- [250] Schutjens PMTM, Spiers CJ. Intergranular pressure solution in NaCl: grain-to-grain contact experiments under the optical microscope. *Rev l'Institut Fr du Pet.* **1999**;54:729–750.
- [251] Urai JL, Schlöder Z, Spiers CJ, et al. Flow and transport properties of salt rocks; 2008; Vol. 60; ISBN 978-3-510-49207-7.
- [252] Kang S-JL. Liquid phase sintering. New York (NY): Springer Science; **2011**; Vol. 39.
- [253] Doremus RH. Glass science. New York (NY): Physics Today; Wiley; **1994**.
- [254] Carter N, Horseman S, Russell J, et al. Rheology of rocksalt. *J Struct Geol.* **1993**;15:1257–1271.
- [255] Kingery WD, Woulbroun JM, Charvat FR. Effects of applied pressure on densification during sintering in the presence of a liquid phase. *J Am Ceram Soc.* **1963**;46:391–395.
- [256] Chen M, Wu S, Xu S, et al. Caking of crystals: characterization, mechanisms and prevention. *Powder Technol.* **2018**;337:51–67.
- [257] Götze J, Möckel R. Quartz: deposits, mineralogy and analytics. Berlin: Springer; **2012**.